LEGIBILITY NOTICE

A major purpose of the Technical Information Center is to provide the broadest dissemination possible of information contained in DOE's Research and Development Reports to business, industry, the academic community, and federal, state and local governments.

Although a small portion of this report is not reproducible, it is being made available to expedite the availability of information on the research discussed herein.

ornl

ORNL/TM-10297

OAK RIDGE
NATIONAL
LABORATORY

MARTIN MARIETTA

Electron-Impact Ionization Data for the Fe Isonuclear Sequence

M. S. Pindzola
D. C. Griffin
C. Bottcher
S. M. Younger
H. T. Hunter

OPERATED BY
MARTIN MARIETTA ENERGY SYSTEMS, INC.
FOR THE UNITED STATES
DEPARTMENT OF ENERGY

ORNL/TM--10297

DE88 003660

Physics Division

ELECTRON-IMPACT IONIZATION DATA FOR THE Fe ISONUCLEAR SEQUENCE

M. S. Pindzola, D. C. Griffin, C. Bottcher,
S. M. Younger, and H. T. Hunter

Date Published - November 1987

Prepared for the
Office of Fusion Energy
U.S. Department of Energy
Washington, DC 20545
Budget Activity No. AT 05 20 26 0

Prepared by the
OAK RIDGE NATIONAL LABORATORY
Oak Ridge, Tennessee 37831
operated by
MARTIN MARIETTA ENERGY SYSTEMS, INC.
for the
U.S. DEPARTMENT OF ENERGY
under contract DE-AC05-840R21400

CONTENTS

ELECTRON-IMPACT IONIZATION DATA FOR THE Fe ISONUCLEAR SEQUENCE

M. S. Pindzola,* D. C. Griffin,† C. Bottcher,
S. M. Younger,§ and H. T. Hunter

ABSTRACT

Collision processes involving highly ionized iron impurities play an important role in magnetically confined fusion plasmas. Available experimental and theoretical cross-section data for electron-impact ionization of ions in the Fe isonuclear sequence in charge states ranging from 1 to 26 are reviewed, and recommended data for each charge state are presented graphically. Contributions to the ionization cross sections due to inner-shell excitation-autoionization have been considered in detail for each ionization stage and make substantial contributions for the intermediate charge states. The role of metastable levels in ionization is also addressed. Maxwellian collisional rate coefficients are calculated from these recommended cross-section data and presented in tabular, graphical, and parametrized form. Comments are made on current research activities leading to future data for Fe ions.

I. INTRODUCTION

The experimental and theoretical study of electron-impact ionization processes in atomic systems has important applications in controlled thermonuclear fusion research.[1,2] Following the discovery that highly charged impurity ions of Mo and W used in tokamak walls and limiters were responsible for rapid line radiation cooling of the plasma, research interest has shifted to lower Z structural materials which generally contain Fe, Ni, and Cr.[3] Accurate electron-ionization atomic data for the atomic ions of the Fe isonuclear sequence has led and will lead to a better understanding of high temperature plasma cooling, transport, and confinement in not only tokamaks but other experimental fusion devices.

In the last decade experiment and theory have shown[4] that indirect resonance processes may make substantial contributions to the electron-impact ionization of transition metal ions especially in low stages of ionization. Contributions to the electron-impact single ionization cross section can be made by the following processes,

$$e^- + A^{q+} \rightarrow A^{(q+1)+} + e^- + e^- \ , \tag{1}$$

$$e^- + A^{q+} \rightarrow [A^{q+}]^* + e^- \ , \qquad [A^{q+}]^* \rightarrow A^{(q+1)+} + e^- \tag{2}$$

and

$$e^- + A^{q+} \rightarrow [A^{(q-1)+}]^* \begin{cases} \longrightarrow [A^{q+}]^* + e^- \\ \qquad \longrightarrow A^{(q+1)+} + e^- \end{cases} , \tag{3}$$

where A represents an arbitrary ion with charge q. The first process is called direct ionization, the second excitation-autoionization and the third resonant-recombination double autoionization. Although a complete quantum mechanical description of electron ionization would include the wave-particle interference between these processes, for the purpose of obtaining a total cross section or rate they can generally be assumed to be independent of one another. Contributions to the electron-impact double ionization cross section can be made by the following processes,

$$e^- + A^{q+} \rightarrow A^{(q+2)+} + e^- + e^- + e^- , \tag{4}$$

and

$$e^- + A^{q+} \rightarrow [A^{(q+1)+}]^* + e^- + e^- \begin{cases} \\ \longrightarrow A^{(q+2)+} + e^- \end{cases} . \tag{5}$$

The first process is called direct double ionization and the second ionization-autoionization. The further processes of excitation-double autoionization and resonant-recombination triple autoionization can also in principle contribute to the double ionization cross section.

The sequential ionization processes summarized in Eqs. (2), (3), and (5) depend critically on the branching ratio found at each step. For example, the doubly excited ion $[A^{q+}]^*$ found in Eq. (2) may radiatively decay to a true bound state of A^{q+} and thus not contribute to single ionization. For low stages of ionization one may generally assume that radiative branching is negligible. For high stages of ionization radiative branching may effectively eliminate many sequential ionization processes. For the double autoionization processes of Eq. (3) one must consider the branching ratio between autoionizing transitions found at the first step. For example, the doubly excited ion $[A^{(q-1)+}]^*$ found in Eq. (3) may decay by autoionizing to a true bound state of A^{q+} and thus not contribute to single ionization. In some cases this is precisely what happens, thus eliminating the resonant-recombination process as an ionization mechanism.

The sequential ionization processes also depend critically on the interaction time. For example the direct process of Eq. (1) occurs on a time scale of 10^{-17} sec, which is approximately the electron-ion collision transit time. The sequential ionization processes all depend on the lifetimes of resonant autoionizing states. Generally these lifetimes range from 10^{-10} sec to 10^{-14} sec. However, sometimes metastable autoionizing states are formed with lifetimes of 10^{-6} sec or longer. Crossed-beams experiments may have scattering chamber to detector ion beam transit times which are faster than 10^{-6} sec, thus eliminating a certain metastable sequential ionization process as an ionization mechanism.

Recently experimental crossed-beams measurements have been made of electron-impact ionization cross sections of ions in the Fe isonuclear sequence.[5-8] Due to the formation characteristics of the ion sources, ion beam currents generally become smaller for the higher ionization stages of a given element. More specifically the ORNL ECR ion source and crossed-beams apparatus has been used to make measurements up to Fe^{15+}. Thus comparison between experiment and theory is currently taking place in the low to intermediate ionization stages of Fe.

II. AVERAGE-CONFIGURATION STATISTICAL MODEL

The direct ionization and excitation-autoionization processes of Eqs. (1) and (2) may be calculated using the average-configuration distorted-wave method. The most general direct ionization transition between configurations is of the form

$$(n_1\ell_1)^{q_1+1}\ k_i\ell_i \rightarrow (n_1\ell_1)^{q_1}\ k_e\ell_e\ k_f\ell_f \quad , \tag{6}$$

where n is the principal number, ℓ is the angular-momentum quantum number, q is the occupation number, and k is the linear momentum wavenumber. The average-configuration direct ionization cross section (in atomic units) is given by[9,10]

$$\sigma_{ion} = \int_0^{E/2} \frac{32(q_1+1)}{k_i^3 k_e k_f} \sum_{\ell_i,\ell_e,\ell_f} (2\ell_i+1)(2\ell_e+1)(2\ell_f+1)M(ef;1i)\ d(k_e^2/2) \quad , \tag{7}$$

where $E = (k_e^2 + k_f^2)/2$. The factor M in Eq. (7) is given by

$$M(ef;1i) = \sum_{\lambda} \begin{pmatrix} \ell_1 & \lambda & \ell_e \\ 0 & 0 & 0 \end{pmatrix}^2 \begin{pmatrix} \ell_i & \lambda & \ell_f \\ 0 & 0 & 0 \end{pmatrix}^2 \frac{[R^{\lambda}(ef;1i)]^2}{(2\lambda+1)}$$

$$+ \sum_{\lambda'} \begin{pmatrix} \ell_1 & \lambda' & \ell_f \\ 0 & 0 & 0 \end{pmatrix}^2 \begin{pmatrix} \ell_i & \lambda' & \ell_e \\ 0 & 0 & 0 \end{pmatrix}^2 \frac{[R^{\lambda'}(fe;1i)]^2}{(2\lambda'+1)}$$

$$-\text{abs} \sum_{\lambda} \sum_{\lambda'} \begin{Bmatrix} \ell_1 & \ell_e & \lambda \\ \ell_i & \ell_f & \lambda' \end{Bmatrix} \begin{pmatrix} \ell_1 & \lambda & \ell_e \\ 0 & 0 & 0 \end{pmatrix} \begin{pmatrix} \ell_i & \lambda & \ell_f \\ 0 & 0 & 0 \end{pmatrix} \begin{pmatrix} \ell_1 & \lambda' & \ell_f \\ 0 & 0 & 0 \end{pmatrix} \begin{pmatrix} \ell_i & \lambda' & \ell_e \\ 0 & 0 & 0 \end{pmatrix}$$

$$\times R^{\lambda}(ef;1i)\, R^{\lambda'}(fe;1i) \quad , \qquad (8)$$

where $R^{\lambda}(ef;1i)$ is the usual Slater radial integral and angular coefficients are summarized in terms of standard 3-j and 6-j symbols. Although there is no rigorous justification for the choice of phase between the direct and exchange scattering amplitudes, the maximum interference approximation[11] is used.

The most general excitation transition between configurations is of the form

$$(n_1\ell_1)^{q_1+1}\, (n_2\ell_2)^{q_2-1}\, k_i\ell_i \rightarrow (n_1\ell_1)^{q_1}\, (n_2\ell_2)^{q_2}\, k_f\ell_f \quad . \qquad (9)$$

The average-configuration excitation cross section is given by

$$\sigma_{exc} = \frac{8\pi}{k_i^3 k_f} (q_1+1)\, (4\ell_2+3-q_2) \sum_{\ell_i,\ell_f} (2\ell_i+1)(2\ell_f+1) M(2f;1i) \quad . \qquad (10)$$

The factor M in Eq. (10) is given by

$$M(2f;1i) = \sum_{\lambda} \begin{pmatrix} \ell_1 & \lambda & \ell_2 \\ 0 & 0 & 0 \end{pmatrix}^2 \begin{pmatrix} \ell_i & \lambda & \ell_f \\ 0 & 0 & 0 \end{pmatrix}^2 \frac{[R^{\lambda}(2f;1i)]^2}{(2\lambda+1)}$$

$$+ \sum_{\lambda'} \begin{pmatrix} \ell_1 & \lambda' & \ell_f \\ 0 & 0 & 0 \end{pmatrix}^2 \begin{pmatrix} \ell_i & \lambda' & \ell_2 \\ 0 & 0 & 0 \end{pmatrix}^2 \frac{[R^{\lambda'}(f2;1i)]^2}{(2\lambda'+1)}$$

$$- \sum_{\lambda} \sum_{\lambda'} (-1)^{\lambda+\lambda'} \begin{Bmatrix} \ell_1 & \ell_2 & \lambda \\ \ell_i & \ell_f & \lambda' \end{Bmatrix} \begin{pmatrix} \ell_1 & \lambda & \ell_2 \\ 0 & 0 & 0 \end{pmatrix} \begin{pmatrix} \ell_i & \lambda & \ell_f \\ 0 & 0 & 0 \end{pmatrix} \begin{pmatrix} \ell_1 & \lambda' & \ell_f \\ 0 & 0 & 0 \end{pmatrix} \begin{pmatrix} \ell_i & \lambda' & \ell_2 \\ 0 & 0 & 0 \end{pmatrix}$$

$$\times R^{\lambda}(2f;1i)\, R^{\lambda'}(f2;1i) \quad . \qquad (11)$$

The continuum normalization in both Eqs. (7) and (10) is chosen as one times a sine function. The bound state orbitals needed to evaluate the Slater radial integrals can be generated using a Hartree-Fock wavefunction code such as the one developed by Cowan.[12] The continuum state orbitals are obtained by solving the radial Schrodinger equation in the distorted-wave approximation. For rapid evaluation of many continuum orbitals a local distorting potential constructed in a semiclassical exchange approximation[13] has proved useful.

The average-configuration distorted wave method can be extended with little more effort to take into account the energy level spread within each configuration. A simple procedure called the average-configuration statistical model (ACSM) is adopted. The average-configuration collision cross section for either the direct ionization or excitation-autoionization process is statistically partitioned over all levels of the final ionized or excited configuration. The total cross section is then summed taking explicit account of the energy position of each level calculated using an atomic-structure program provided by Cowan.[12] If the atomic structure calculations show that certain excited levels are bound, their contribution to the ionization cross section is of course ignored. Branching ratios for autoionization versus radiation are also calculated for each excited level and then multiplied by the statistically partitioned excitation cross sections. A statistically weighted Boltzmann distribution over the levels of the initial configuration, based on an average ion temperature, may also be included in the average-configuration statistical model.

Average-configuration direct ionization cross sections have been calculated for the outer subshells of many of the ground and excited configurations in the Fe isonuclear sequence. For ease in accessing the results of the numerical calculations, the direct cross section for each subshell may be written in the following parametrized form[14]

$$\sigma(E) = \frac{1}{IE}\left[A\left(1 - \frac{I}{E}\right) + B\left(1 - \frac{I}{E}\right)^2 + C\,\ell n\left(\frac{E}{I}\right) + \frac{DI}{E}\,\ell n\left(\frac{E}{I}\right)\right] , \qquad (12)$$

where E is the incident electron energy in eV, I is the subshell ionization potential in eV, and the cross section is in cm^2. A, B, C, D parameters for the ground configuration of all Fe ions are collected together[14-16] and presented in Table I. A, B, C, D parameters for various excited configurations are given in Table II. For those inner subshells not found in Tables I and II, the semiempirical formula due to Lotz[17] can be used to estimate the cross section.

Average-configuration excitation cross sections have been calculated for transitions to many of the autoionizing configurations in the Fe isonuclear sequence. The strongest excitation cross sections for transitions from the ground configuration are presented in Table III, while similar cross sections from the excited configurations are given in Table IV. Additional atomic structure information is presented in Tables III and IV, from which calculations for the total ionization cross section in the average-configuration statistical model can be made.

III. CROSS SECTIONS FOR Fe ATOMIC IONS

In Fig. 1 the crossed-beams measurements of Montague et al.[5] for Fe^+ are compared with an ACSM calculation for the $3p^63d^64s$ ground configuration, which includes the 3p→3d excitation and direct ionization of the 4s and 3d subshells. Near threshold the direct cross sections alone are higher than experiment. Further theoretical investigation into the effects of configuration-interaction and direct-indirect interference are clearly needed.

In Fig. 2 the crossed-beams measurements of Mueller et al.[6] for Fe^{2+} are compared with an ACSM calculation[18] for the $3p^63d^6$ ground configuration, which includes the 3p→3d excitation and direct ionization of the 3d subshell. The total and direct cross sections bracket the experiment over a wide energy range. Very near threshold the experimental measurements clearly indicate the contribution of metastable states within the ground configuration. The 3p→4p excitation (not included) would further increase the calculated indirect contribution to the total ionization cross section by 20%. Atomic structure calculations indicate that most of the levels, 173 out of 180, of the $3p^53d^6$ configuration formed by direct ionization of the 3p shell are autoionizing. Thus most of the 3p direct ionization contributes to the double ionization of Fe^{2+}.

In Fig. 3 an ACSM calculation[18] for the $3p^63d^5$ ground configuration of Fe^{3+}, including the 3p→3d excitation-autoionization contribution and direct ionization of the 3d and 3p subshells, is presented. Atomic structure calculations indicate that only a few of the levels, 31 out of 214, of the $3p^53d^5$ configuration formed by direct ionization of the 3p shell are autoionizing. Thus most of the 3p direct ionization contributes to the single ionization of Fe^{3+}.

In Fig. 4 an ACSM calculation for the $3p^63d^4$ ground configuration of Fe^{4+}, including 9 different excitations and direct ionization of the 3d, 3p, and 3s subshells, is presented. The 3p→3d excitation creates the same final configuration as discussed in the previous paragraph for 3p ionization of Fe^{3+}. Since only 31 out of the 214 levels are autoionizing, the 3p→3d contributions become relatively small. The 3p→4p excitation is comparable in magnitude to the 3p→3d excitation since all 1038 levels of the $3p^53d^44p$ configuration are autoionizing. The 3s→3d and 3p→4d excitations are also quite important.

In Fig. 5 the crossed-beams measurements of Gregory et al.[7] for Fe^{5+} are compared with an ACSM calculation[19] for the $3p^63d^3$ ground configuration which includes 10 different excitations and direct ionization of the 3d, 3p, and 3s subshells. The 3p→4p excitation is the strongest, but important contributions are made by the 3s→3d and 3p→4d excitations. Beyond the 10 specific excitations included, an n^3 rule extrapolation was used to approximate the remaining non-negligible 3p→nℓ excitation-autoionization contributions. The agreement between theory and experiment is reasonably good. The smooth appearance of the theoretical curve results from the statistical partition of the total excitation collision cross section over more than 5000 levels. An ACSM calculation[19] for Fe^{5+} was repeated for electron ionization of the $3p^63d^24s$ excited configuration, including 10 different excitations and direct ionization of the 4s, 3d, and 3p subshells. In Fig. 6 the theoretical curve for the excited configuration is larger than that for the ground configuration because of the additional presence of the strong 3p→3d excitation. From the poor agreement found between experiment and theory in Fig. 6, one concludes that most of the metastable states in the excited configuration have decayed during the ion beam time of flight from source to scattering chamber.

In Fig. 7 the crossed-beams measurements of Gregory et al.[7] for Fe^{6+} are compared with an ACSM calculation[19] for the $3p^63d^2$ ground configuration, which includes 9 different excitations and direct ionization of the 3d, 3p, and 3s subshells. The 3p→4p excitation is reduced in strength, due to the fact that only 24 of the 256 levels of the $3p^53d^24p$ configuration are autoionizing. The 3p→4f excitation is the strongest, but important contributions are made by the 3s→4s and 3p→5ℓ excitations. Higher 3p→nℓ excitations are estimated using the n^3 rule. An ACSM calculation[19] for Fe^{6+} was repeated for electron ionization of the $3p^63d4s$ excited configuration including 9 different excitations and direct ionization of the 4s, 3d, 3p, and 3s subshells. In Fig. 8 the agreement between theory and experiment is poor, again indicating that a substantial number of metastable states in the excited configuration have decayed before the measurements are made.

In Fig. 9 an ACSM calculation for the $3p^63d$ ground configuration of Fe^{7+}, including 10 different excitations and direct ionization of the 3d, 3p, and 3s subshells, is presented. The 3p→5ℓ and 3s→4ℓ excitations are the most important and higher nℓ excitations are estimated using the n^3 rule.

In Fig. 10 an ACSM calculation for the $3s^23p^6$ ground configuration of Fe^{8+}, including the 2p→3d excitation and direct ionization of the 3p and 3s subshells, is presented. An ACSM calculation for the $3s^23p^53d$ excited configuration, including 10 different excitations and direct ionization of the 3d, 3p, and 3s subshells, is shown in Fig. 11. The 2p→3d excitation is the strongest, but important contributions are made by 3s→4ℓ excitations.

In Fig. 12 the crossed-beams measurements of Gregory et al.[7] for Fe^{9+} are compared with an ACSM calculation[19] for the $3s^23p^5$ ground configuration, which includes the 2p→3d excitation and direct ionization of the 3p and 3s subshells. The theory falls below experiment and does not predict the proper threshold energy. An ACSM calculation[19] for Fe^{9+} was repeated for electron ionization of the $3s^23p^43d$ excited configuration, including 5 different excitations and direct ionization of the 3d, 3p, and 3s subshells. The 2p→3d excitation is the strongest, but important contributions are made by 3s→4ℓ excitations. In Fig. 13 the agreement between theory and experiment has improved. It seems that the experiment on Fe^{9+} is predominately measuring electron ionization from the metastable states of the excited configuration.

In Fig. 14 an ACSM calculation for the $3s^23p^4$ ground configuration of Fe^{10+}, including 5 different excitations and direct ionization of the 3p and 3s subshells, is presented. The 2p→3d excitation is the strongest, but important contributions are made by the 2p→3p and 2s→3d excitations. An ACSM calculation for the $3s^23p^33d$ excited configuration, including 10 different excitations and direct ionization of the 3d, 3p, and 3s subshells, is shown in Fig. 15. The 2p→3d excitation is the strongest, but contributions are made by 3s→5ℓ excitations.

In Fig. 16 the crossed-beams measurements of Gregory et al.[8] for Fe^{11+} are compared with an ACSM calculation[19] for the $3s^23p^3$ ground configuration, which includes 5 different excitations and direct ionization of the 3p and 3s subshells. The theory falls below experiment and does not predict the proper threshold energy. An ACSM calculation for Fe^{11+} was repeated for electron ionization of the $3s^23p^23d$ excited configuration, including 10 different excitations and direct ionization of the 3d, 3p, and 3s subshells. The 2p→3d excitation is the strongest, but contributions are made by 3s→5ℓ and 2p→3p excitations. In Fig. 17 the agreement between theory and experiment has markedly improved, but the contributions from the lower energy 3s→5ℓ excitations seems to be theoretically overestimated. It is surprising that the experiment apparently shows a large fraction of initial ions in the $3s^53p^23d$ configuration when only a small fraction of the states of this configuration should be metastable.

In Fig. 18 an ACSM calculation for the $3s^23p^2$ ground configuration of Fe^{12+}, including 5 different excitations and direct ionization of the 3p and 3s subshells, is presented. The 2p→3d excitation is the strongest, but important contributions are made by 2p→3p and 2s→3d excitations.

In Fig. 19 the crossed-beams measurements of Gregory et al.[8] for Fe^{13+} are compared with an ACSM calculation[19] for the $3s^23p$ ground configuration, which includes 5 different excitations and direct ionization of the 3p and 3s subshells. With the scatter of experimental points it is difficult to make a definitive judgment of the theory.

In Fig. 20 an ACSM calculation for the $2p^6 3s^2$ ground configuration of Fe^{14+}, including 8 different excitations and direct ionization of the 3s subshell, is presented. The 2p→3d excitation is the strongest, but important contributions are made by the 2p→3p and 2s→3d excitations. An ACSM calculation for the $2p^6 3s3p$ excited configuration, including 9 different excitations and direct ionization of the 3p, 3s, and 2p subshells, is shown in Fig. 21. The 2p→3p and 2p→3d are the strongest excitations. Radiative branching has a significant effect on the 2p→3d excitation in both cases. Therefore, there is more uncertainty in the theoretical calculations for this ion due to errors inherent in averaging over branching ratios with the ACSM.

In Fig. 22 the crossed-beams measurements of Gregory et al.[8] for Fe^{15+} are compared with an average-configuration distorted-wave calculation[20] for the $2p^6 3s$ ground configuration. Although the 2p→3d excitation cross section is the largest, the branching ratio for autoionization is only 1/3. Both the 2p→3p and 2s→3d excitations, with branching ratios for autoionization close to unity, are also sizable. Contributions from resonant-recombination double autoionization, see Eq. (3), which are predicted to increase the ionization rate at certain temperatures by as much as 20%, appear to be missing in the experimental data.

For Fe^{16+} through Fe^{23+} the contributions of excitation-autoionization to the total ionization cross section should be fairly small. For electron ionization from the ground configuration, the direct cross section results of Table I should give a reasonable estimate of the total cross section. Theoretical calculations have been made which investigate excitation-autoionization contributions to the single ionization of the Fe^{23+} atomic ion.[21] Although the 1s→2s and 1s→2p excitation cross sections are about 20% of the direct cross section, the branching ratio for autoionization is quite small. The overall enhancement of the total ionization cross section due to excitation-autoionization is estimated to be only about 3%. We note that the role of metastable states in excited configurations is not yet fully understood for electron ionization of highly ionized iron.

IV. RATE COEFFICIENTS FOR Fe ATOMIC IONS

Rate coefficients for Fe^{+} through Fe^{25+} were calculated using the theoretical and experimental cross section data discussed in the previous section. The theoretical results are presented in Tables V-X and Figs. 23-28, while the experimental results are presented in Table XI and Fig. 29. In addition to the tabulated values, a set of fitting parameters are included which allows the user to calculate the rate coefficient at any value of kT from E_{min} to E_{max} = 20 keV (where E_{min} is listed in the tables) for any of the ions included here. The coefficients A_0 through A_6 in Tables V-XI were fitted following the method reported by Cox and Hayes[22] and may be utilized in a direct expansion through Chebychev polynomials of the first kind $[T_n(x)]$[23] to obtain rate coefficients through the formula

$$\alpha(kT) = A_0/2 + \sum_{n=1}^{6} A_n \, T_n(x) \quad , \tag{13}$$

where the reduced energy x is given by

$$x = \frac{[2\ell n(kT) - \ell n(E_{max}) - \ell n(E_{min})]}{\ell n(E_{max}) - \ell n(E_{min})} \quad , \; kT \text{ and } E_{min} \text{ in (eV)} \; ; \tag{14}$$

$E_{max} = 20{,}000$ eV .

Our recommendation for Fe isonuclear rate coefficients is to use the experimental results for Fe^{+}, Fe^{2+}, Fe^{5+}, Fe^{6+}, Fe^{9+}, Fe^{11+}, Fe^{13+}, and Fe^{15+}; the theoretical results for Fe^{3+}, Fe^{4+}, Fe^{7+}, Fe^{8+*}, Fe^{10+*}, Fe^{12+}, and Fe^{14+*}; and the direct ionization results from Table I for Fe^{16+} through Fe^{25+}. These recommended rates are incorporated in a subroutine called FERATE (Q, TEMP), which will return the rate coefficient in cm^3/sec for any ionic charge Q and temperature, TEMP, in electron volts. It will be available as a library function at the National Magnetic Fusion Energy Computer Center in Livermore, California. A listing of a program, written in Basic, that produces rates using the given Chebyshev coefficients is found in Table XII.

V. CONCLUSIONS

In summary we have learned a great deal by examining electron-impact ionization along the Fe isonuclear sequence. Although directly applicable to numerical studies of transport phenomena in plasmas, an isonuclear series presents additional theoretical complications due to the changing atomic structure. Cross sections and branching ratios are not amenable to scaling along an isonuclear sequence. Sequential ionization processes, such as excitation-autoionization, can be relatively large for several ionization stages, become almost negligible and then reappear at higher stages of ionization. Multiple ionization may also be important, especially when the ionization-autoionization process involves an almost filled subshell. Current comparisons of experimental crossed-beams measurements and theory are complicated by the presence of a substantial, but unknown, fraction of metastable states in the ion beam. The future study of the electron-impact ionization of metastable states of excited configurations promises to provide further insight into our understanding of the ionization processes found in the high temperature plasmas of controlled fusion devices.

ACKNOWLEDGMENTS

We would like to thank all the members of the ORNL experimental group, in particular D. C. Gregory and R. A. Phaneuf, for many valuable discussions. We also would like to acknowledge R. D. Cowan for providing us with a copy of his atomic-structure programs and a number of helpful conversations.

REFERENCES

*Department of Physics, Auburn University, Auburn, Alabama 36849.
†Department of Physics, Rollins College, Winter Park, Florida 32789.
§Department of Defense Science, Lawrence Livermore Laboratory, Livermore, California 94550.

1. M.R.C. McDowell and A. M. Ferendeci, eds. of "Atomic and Molecular Processes in Controlled Thermonuclear Fusion," NATO ASI B53 (Plenum, New York, 1980).
2. C. J. Joachain and D. E. Post, eds. of "Atomic and Molecular Physics of Controlled Thermonuclear Fusion," NATO ASI B101 (Plenum, New York, 1983).
3. C. F. Barnett, Nucl. Instrum. Methods 214, 1 (1983).
4. D. H. Crandall in "Physics of Electron and Atomic Collisions; Invited Papers of the XII ICPEAC," ed. S. Datz (North-Holland, Amsterdam, 1982), p. 595.
5. R. G. Montague, M. J. Diserens, and M.F.A. Harrison, J. Phys. B 17, 2085 (1984). [Fe^{+}]
6. D. W. Mueller, T. J. Morgan, G. H. Dunn, D. C. Gregory, and D. H. Crandall, Phys. Rev. A 31, 2905 (1985). [Fe^{2+}]
7. D. C. Gregory, F. W. Meyer, A. Müller, and P. Defrance, Phys. Rev. A 34, 3657 (1986). [Fe^{5+}, Fe^{6+}, and Fe^{9+}]
8. D. C. Gregory, L.-J. Wang, F. W. Meyer, and K. Rinn, Phys. Rev. A 35, 3256 (1987). [Fe^{11+}, Fe^{13+}, Fe^{15+}]
9. S. M. Younger, Phys. Rev. A 22, 111 (1980).
10. H. Jakubowicz and D. L. Moores, J. Phys. B 14, 3733 (1981).
11. R. K. Peterkop, Zh. Eksp. Teor. Fiz. 41, 1938 (1961) [Sov. Phys. JETP 14, 1377 (1962)].
12. R. D. Cowan, "The Theory of Atomic Structure and Spectra" (California Press, Berkeley, 1981).
13. M. E. Riley and D. G. Truhlar, J. Chem. Phys. 63, 2182 (1975).
14. S. M. Younger in "Atomic Data for Fusion," eds. D. H. Crandall, C. F. Barnett, and W. L. Wiese, Vol. 7, 190 (1981).
15. S. M. Younger, Phys. Rev. A 24, 1272 (1981).
16. S. M. Younger, J. Quan. Spectrosc. Radiat. Transfer 27, 541 (1982).
17. W. Lotz, Z. Phys. 206, 205 (1967).
18. M. S. Pindzola, D. C. Griffin, C. Bottcher, D. C. Gregory, A. M. Howald, R. A. Phaneuf, D. H. Crandall, G. H. Dunn, D. W. Mueller, and T. J. Morgan, ORNL/TM-9436 (1985). [Fe^{2+}, Fe^{3+}, Fe^{4+}]
19. M. S. Pindzola, D. C. Griffin, and C. Bottcher, Phys. Rev. A 34, 3668 (1986). [Fe^{5+}, Fe^{6+}, Fe^{9+}, Fe^{11+}, Fe^{13+}]

20. K. J. LaGattuta and Y. Hahn, Phys. Rev. A 24, 2273 (1981). [Fe^{15+}]
21. K. Butler and D. L. Moores, J. Phys. B 18, 1247 (1985). [Fe^{23+}]
22. M. G. Cox and J. G. Hayes, "Curve Fitting: A Guide and Suite of Algorithms for the Non-Specialist User," U.K. National Physical Laboratory Report NAC26, December 1973.
23. See, for example, Handbook of Mathematical Functions, eds. Milton Abramowitz and Irene A. Stegun (Dover, New York, 1970), p. 795.

Table I. Direct ionization cross section parameters for ground configurations in units of 10^{-14} $(eV \cdot cm)^2$

Ion	Configuration	Subshell	I(eV)	A	B	C	D
Fe^{+}	$3p^6 3d^6 4s$	4s	14.82	6.58	1.29	0.160	-3.21
		3d	24.83	66.2	-54.6	18.6	-71.1
		3p	83.37	115.0	-72.4	9.57	-107.0
Fe^{2+}	$3s^2 3p^6 3d^6$	3d	34.75	97.5	-67.6	21.0	-103.0
		3p	93.28	87.7	-49.6	11.4	-84.8
		3s	131.9	25.9	-11.7	2.32	-23.9
Fe^{3+}	$3s^2 3p^6 3d^5$	3d	53.74	77.4	-43.9	19.6	-81.9
		3p	111.9	79.1	-30.0	8.38	-74.6
		3s	151.0	16.7	-3.44	2.32	-15.1
Fe^{4+}	$3s^2 3p^6 3d^4$	3d	75.15	48.1	-20.4	16.2	-48.4
		3p	132.7	66.8	-18.9	9.29	-60.5
		3s	172.4	13.4	-0.410	2.33	-10.9
Fe^{5+}	$3s^2 3p^6 3d^3$	3d	98.69	36.9	-11.8	10.3	-31.5
		3p	155.5	67.0	-18.6	9.43	-56.5
		3s	195.8	12.7	-0.0863	2.42	-8.97
Fe^{6+}	$3s^2 3p^6 3d^2$	3d	124.2	14.6	-4.36	5.98	-10.5
		3p	180.0	67.9	-20.6	9.82	-53.7
		3s	220.9	15.6	-2.29	2.30	-10.6
Fe^{7+}	$3s^2 3p^6 3d$	3d	151.7	14.3	-4.44	2.45	-9.53
		3p	206.1	70.3	-23.4	9.89	-53.5
		3s	247.7	18.0	-4.29	2.27	-12.0
Fe^{8+}(Ar)	$3s^2 3p^6$	3p	233.6	71.0	-23.9	9.47	-51.9
		3s	275.9	19.1	-5.55	2.32	-12.7
Fe^{9+}(Cl)	$3s^2 3p^5$	3p	262.1	57.0	-18.6	7.64	-39.7
		3s	305.7	20.8	-7.40	2.28	-14.1
Fe^{10+}(S)	$3s^2 3p^4$	3p	290.3	44.7	-14.4	5.88	-30.1
		3s	325.2	22.3	-8.65	2.22	-15.2
Fe^{11+}(P)	$3s^2 3p^3$	3p	330.8	32.7	-9.73	4.40	-20.9
		3s	368.4	24.7	-10.2	2.27	-17.0
Fe^{12+}(Si)	$3s^2 3p^2$	3p	361.0	20.5	-5.65	2.82	-12.3
		3s	403.0	26.2	-11.3	2.25	-18.2

Table I (Continued)

Ion	Configuration	Subshell	I(eV)	A	B	C	D
Fe^{13+}(Al)	$3s^2 3p$	3p	392.2	9.77	-2.58	1.35	-5.57
		3s	426.0	27.5	-12.0	1.91	-19.3
Fe^{14+}(Mg)	$3s^2$	3s	457.0	38.8	-16.7	1.87	-28.8
Fe^{15+}(Na)	$2s^2 2p^6 3s$	3s	488.9	8.95	-2.62	0.963	-5.34
		2p	1219.0	78.9	-27.2	10.5	-53.0
		2s	1351.0	22.5	-7.80	2.96	-16.5
Fe^{16+}(Ne)	$2s^2 2p^6$	2p	1266.0	50.4	-16.1	4.03	-30.5
		2s	1394.0	11.8	-3.27	1.64	-7.58
Fe^{17+}(F)	$2s^2 2p^5$	2p	1366.0	42.0	-13.4	3.36	-25.4
		2s	1482.0	11.8	-3.27	1.64	-7.58
Fe^{18+}(O)	$2s^2 2p^4$	2p	1463.0	33.6	-10.7	2.69	-20.3
		2s	1566.0	11.8	-3.27	1.64	-7.58
Fe^{19+}(N)	$2s^2 2p^3$	2p	1583.0	25.2	-8.04	2.02	-15.2
		2s	1679.0	11.8	-3.27	1.64	-7.58
Fe^{20+}(C)	$2s^2 2p^2$	2p	1678.0	16.8	-5.3[illegible]	1.34	-10.2
		2s	1755.0	11.8	-3.27	1.64	-7.58
Fe^{21+}(B)	$2s^2 2p$	2p	1789.0	8.40	-2.68	0.672	-5.08
		2s	1852.0	11.8	-3.27	1.64	-7.58
Fe^{22+}(Be)	$2s^2$	2s	1950.0	11.8	-3.27	1.64	-7.58
Fe^{23+}(Li)	$1s^2 2s$	2s	2046.0	5.90	-1.64	0.820	-3.79
		1s	8694.0	15.0	-5.21	2.39	-12.3
Fe^{24+}(He)	$1s^2$	1s	8829.0	15.0	-5.21	2.39	-12.3
Fe^{25+}(H)	1s	1s	9277.0	7.50	-2.61	1.20	-6.15

Table II. Direct ionization cross section parameters for excited configurations in units of 10^{-14} $(eV \cdot cm)^2$

Ion	Configuration	Subshell	I(eV)	A	B	C	D
Fe^{5+}	$3s^2 3p^6 3d^2 4s$	4s	66.20	9.35	-3.34	0.432	-5.61
		3d	107.65	18.70	-6.22	8.55	-16.09
Fe^{6+}	$3s^2 3p^6 3d 4s$	4s	81.78	7.40	-2.04	0.496	-3.82
		3d	134.27	10.33	-3.14	3.64	-7.39
Fe^{8+} (Ar)	$3s^2 3p^5 3d$	3d	178.79	12.11	-3.58	2.55	-7.19
		3p	234.49	53.73	-17.18	9.21	-39.11
		3s	276.07	17.81	-4.79	2.50	-12.00
Fe^{9+} (Cl)	$3s^2 3p^4 3d$	3d	207.86	12.70	-3.74	2.10	-7.09
		3p	263.66	44.05	-14.58	7.19	-31.17
		3s	303.11	18.06	-5.26	2.44	-11.85
Fe^{10+} (S)	$3s^2 3p^3 3d$	3d	238.07	13.08	-3.83	1.74	-7.00
		3p	293.79	32.80	-10.77	5.21	-22.41
		3s	330.98	16.76	-4.70	2.38	-10.31
Fe^{11+} (P)	$3s^2 3p^2 3d$	3d	269.40	13.25	-3.84	1.45	-6.84
		3p	324.87	21.10	-6.65	3.34	-13.75
		3s	359.66	14.98	-3.81	2.31	-8.35
Fe^{14+} (Mg)	$2p^6 3s 3p$	3p	421.63	8.70	-2.15	1.43	-4.51
		3	457.88	8.77	-2.95	1.10	-5.20
		2p	1173.67	73.90	-24.51	12.12	-50.15

Table III. Strongest excitation cross section for ground configurations in units of 10^{-18} cm^2

Ion	Transition	Initial Configuration	Number of Bound Levels	Energy Spread (eV)	Final Configuration	Number of Bound Levels	Number of Autoionizing Levels	Energy Spread (eV)	Average Excitation Energy (eV)	Threshold Cross Section (10^{-18} cm^2)	Twice Threshold Cross Section (10^{-18} cm^2)
Fe^{+}	3p→3d	$3p^6 3d^6 4s$	63	15.10	$3p^5 3d^7 4s$	0	213	29.14	57.84	35.[illegible]	18.04
Fe^{2+}	3p→3d	$3p^6 3d^6$	34	14.89	$3p^5 3d^7$	0	110	29.02	57.28	28.[illegible]	19.96
Fe^{3+}	3p→3d	$3p^6 3d^5$	37	15.98	$3p^5 3d^6$	7	173	34.50	57.52	32.22	27.64
Fe^{4+}	3p→3d	$3p^6 3d^4$	34	17.76	$3p^5 3d^5$	183	31	43.78	57.53	44.65	35.76
Fe^{5+}	3p→4p	$3p^6 3d^3$	19	10.48	$3p^5 3d^3 4p$	194	419	37.31	98.52	4.85	2.79
Fe^{6+}	3p→4f	$3p^6 3d^2$	9	9.72	$3p^5 3d^2 4f$	0	472	31.66	136.56	1.104	0.647
Fe^{7+}	3p→5p	$3p^6 3d$	2	0.22	$3p^5 3d 5p$	1	64	26.58	156.88	0.828	0.427
Fe^{8+}	2p→3d	$3s^2 3p^6$	1	0.00	$2p^5 3s^2 3p^6 3d$	0	12	19.92	739.01	0.180	0.113
Fe^{9+}	2p→3d	$3s^2 3p^5$	2	1.89	$2p^5 3s^2 3p^5 3d$	0	65	44.28	746.89	0.187	0.119
Fe^{10+}	2p→3d	$3s^2 3p^4$	5	11.48	$2p^5 3s^2 3p^4 3d$	0	158	51.13	755.16	0.194	0.124
Fe^{11+}	2p→3d	$3s^2 3p^3$	5	11.32	$2p^5 3s^2 3p^3 3d$	0	203	54.12	763.80	0.201	0.130
Fe^{12+}	2p→3d	$3s^2 3p^2$	5	12.80	$2p^5 3s^2 3p^2 3d$	0	158	49.61	772.81	0.207	0.135
Fe^{13+}	2p→3d	$3s^2 3p$	2	2.28	$2p^5 3s^2 3p 3d$	0	65	41.46	782.20	0.213	0.140
Fe^{14+}	2p→3d	$2p^6 3s^2$	1	0.00	$2p^5 3s^2 3d$	0	12	24.29	791.95	0.218	0.144

Table IV. Strongest excitation cross section for excited configurations in units of 10^{-18} cm^2

Ion	Transition	Initial Configuration	Number of Bound Levels	Energy Spread (eV)	Final Configuration	Number of Bound Levels	Number of Autoionizing Levels	Energy Spread (eV)	Average Excitation Energy (eV)	Threshold Cross Section (10^{-18} cm^2)	Twice Threshold Cross Section (10^{-18} cm^2)
Fe^{5+}	3p→3d	$3p^6 3d^2 4s$	16	9.91	$3p^5 3d^3 4s$	161	52	36.64	57.48	73.75	49.51
Fe^{6+}	3p→4p	$3p^6 3d 4s$	4	0.80	$3p^5 3d 4s 4p$	0	130	33.81	114.86	4.40	2.39
Fe^{8+}	2p→3d	$3s^2 3p^5 3d$	12	26.12	$2p^5 3s^2 3p^5 3d^2$	0	256	53.72	740.17	0.161	0.100
Fe^{9+}	2p→3d	$3s^2 3p^4 3d$	28	28.46	$2p^5 3s^2 3p^4 3d^2$	0	604	72.88	747.94	0.167	0.106
Fe^{10+}	2p→3d	$3s^2 3p^3 3d$	38	33.08	$2p^5 3s^2 3p^3 3d^2$	0	808	77.03	756.09	0.173	0.111
Fe^{11+}	2p→3d	$3s^2 3p^2 3d$	28	24.90	$2p^5 3s^2 3p^2 3d^2$	0	604	68.73	764.63	0.179	0.115
Fe^{14+}	2p→3d	$2p^6 3s 3p$	4	17.51	$2p^5 3s 3p 3d$	0	130	53.75	791.02	0.218	0.144

Table V. Theoretical Electron-Impact Ionization Rate Coefficients for $e^- + Fe^{q+} \rightarrow Fe^{(q+1)+} + 2e^-$

Maxwellian Rate Coefficients (cm^3/s)

e^- Temp. (eV)	Fe^+	Fe^{2+}	Fe^{3+}	Fe^{4+}	Fe^{5+}	Fe^{5+*}
1.0E+00	3.66E-17	7.64E-25	7.04E-33	0.00E+00	0.00E+00	5.82E-38
2.0E+00	7.95E-13	7.74E-17	1.10E-20	1.31E-25	2.55E-30	3.07E-23
4.0E+00	1.69E-10	1.13E-12	1.69E-14	4.57E-17	1.69E-19	7.45E-16
7.0E+00	2.02E-09	8.76E-11	8.52E-12	2.24E-13	7.93E-15	1.10E-12
1.0E+01	5.79E-09	5.53E-10	1.07E-10	6.99E-12	6.08E-13	2.04E-11
2.0E+01	2.20E-08	5.44E-09	2.16E-09	4.15E-10	1.03E-10	6.37E-10
4.0E+01	4.63E-08	1.88E-08	1.03E-08	3.39E-09	1.40E-09	3.72E-09
7.0E+01	6.51E-08	3.31E-08	2.07E-08	8.55E-09	4.35E-09	8.04E-09
1.0E+02	7.44E-08	4.18E-08	2.76E-08	1.25E-08	6.88E-09	1.09E-08
2.0E+02	8.45E-08	5.42E-08	3.82E-08	1.94E-08	1.15E-08	1.55E-08
4.0E+02	8.51E-08	5.87E-08	4.30E-08	2.31E-08	1.36E-08	1.75E-08
7.0E+02	8.07E-08	5.65E-08	4.22E-08	2.30E-08	1.35E-08	1.69E-08
1.0E+03	7.64E-08	5.32E-08	3.99E-08	2.18E-08	1.28E-08	1.56E-08
2.0E+03	6.56E-08	4.47E-08	3.38E-08	1.83E-08	1.08E-08	1.26E-08
4.0E+03	5.35E-08	3.57E-08	2.70E-08	1.45E-08	8.62E-09	9.79E-09
7.0E+03	4.31E-08	2.84E-08	2.20E-08	1.18E-08	6.97E-09	7.84E-09
1.0E+04	3.57E-08	2.34E-08	1.90E-08	1.02E-08	5.91E-09	6.73E-09
2.0E+04	2.10E-08	1.38E-08	1.31E-08	6.99E-09	3.74E-09	4.70E-09

Chebychev Fitting Parameters for Rate Coefficients

	E_{min} (eV)	E_{max} (eV)	A0	A1	A2	A3	A4	A5	A6
Fe^+	2.0	2.0E+04	7.278E-08	2.083E-08	-3.336E-08	-1.068E-08	1.149E-08	3.042E-10	-4.061E-09
Fe^{2+}	4.0	2.0E+04	4.772E-08	1.338E-08	-2.234E-08	-7.187E-09	7.477E-09	7.001E-10	-2.110E-09
Fe^{3+}	7.0	2.0E+04	3.775E-08	1.010E-08	-1.657E-08	-3.030E-09	6.101E-09	-5.628E-10	-1.889E-09
Fe^{4+}	7.0	2.0E+04	1.917E-08	5.805E-09	-8.352E-09	-2.613E-09	3.118E-09	3.128E-10	-8.449E-10
Fe^{5+}	10.	2.0E+04	1.164E-08	3.150E-09	-5.229E-09	-1.118E-09	2.071E-09	-1.741E-10	-8.048E-10
Fe^{5+*}	7.0	2.0E+04	1.434E-08	3.619E-09	-6.726E-09	-1.135E-09	2.696E-09	-1.961E-10	-8.510E-10

Table VI. Theoretical Electron-Impact Ionization Rate Coefficients for $e^- + Fe^{q+} \rightarrow Fe^{(q+1)+} + 2e^-$

Maxwellian Rate Coefficients (cm^3/s)

e^- Temp. (eV)	Fe^{6+}	Fe^{6+*}	Fe^{7+}	Fe^{8+}	Fe^{8+*}	Fe^{9+}	Fe^{9+*}
1.0E+00	0.00E+00	0.00E+00	0.00E+00	0.00E+00	0.00E+00	0.00E+00	0.00E+00
2.0E+00	3.40E-37	2.49E-28	0.00E+00	0.00E+00	0.00E+00	0.00E+00	0.00E+00
4.0E+00	5.41E-23	8.26E-19	8.49E-26	4.31E-36	2.79E-29	1.73E-39	2.97E-32
7.0E+00	7.12E-17	1.39E-14	1.84E-18	1.11E-24	7.13E-21	1.13E-26	1.00E-22
1.0E+01	2.05E-14	7.71E-13	1.55E-15	4.13E-20	1.79E-17	1.53E-21	7.15E-19
2.0E+01	1.52E-11	9.33E-11	3.80E-12	9.61E-15	1.94E-13	1.59E-15	2.68E-14
4.0E+01	4.12E-10	1.09E-09	1.81E-10	5.22E-12	2.43E-11	1.81E-12	6.67E-12
7.0E+01	1.71E-09	3.14E-09	9.43E-10	8.39E-11	2.15E-10	3.99E-11	8.43E-11
1.0E+02	3.03E-09	4.81E-09	1.83E-09	2.63E-10	5.38E-10	1.42E-10	2.47E-10
2.0E+02	5.77E-09	7.69E-09	3.97E-09	1.04E-09	1.64E-09	6.55E-10	9.31E-10
4.0E+02	7.32E-09	8.97E-09	5.54E-09	2.05E-09	2.86E-09	1.42E-09	1.84E-09
7.0E+02	7.43E-09	8.79E-09	5.94E-09	2.59E-09	3.43E-09	1.89E-09	2.36E-09
1.0E+03	7.11E-09	8.31E-09	5.82E-09	2.71E-09	3.53E-09	2.03E-09	2.50E-09
2.0E+03	6.07E-09	6.99E-09	5.12E-09	2.58E-09	3.30E-09	2.00E-09	2.42E-09
4.0E+03	4.89E-09	5.59E-09	4.18E-09	2.19E-09	2.77E-09	1.72E-09	2.07E-09
7.0E+03	3.96E-09	4.52E-09	3.41E-09	1.82E-09	2.31E-09	1.44E-09	1.74E-09
1.0E+04	3.36E-09	3.83E-09	2.90E-09	1.55E-09	2.02E-09	1.23E-09	1.53E-09
2.0E+04	2.13E-09	2.42E-09	1.84E-09	9.92E-10	1.52E-09	7.89E-10	1.15E-09

Chebychev Fitting Parameters for Rate Coefficients

	E_{min} (eV)	E_{max} (eV)	A0	A1	A2	A3	A4	A5	A6
Fe^{6+}	10.	2.0E+04	6.231E-09	1.889E-09	-2.698E-09	-8.721E-10	1.100E-09	4.342E-11	-4.575E-10
Fe^{6+*}	7.0	2.0E+04	7.194E-09	2.194E-09	-3.221E-09	-1.139E-09	1.155E-09	1.651E-10	-3.116E-10
Fe^{7+}	10.	2.0E+04	4.886E-09	1.684E-09	-1.980E-09	-9.566E-10	7.099E-10	1.967E-10	-2.480E-10
Fe^{8+}	20.	2.0E+04	2.335E-09	8.727E-10	-8.580E-10	-4.906E-10	2.725E-10	1.161E-10	-8.374E-11
Fe^{8+*}	20.	2.0E+04	3.198E-09	1.149E-09	-1.127E-09	-4.709E-10	4.324E-10	8.121E-11	-1.453E-10
Fe^{9+}	20.	2.0E+04	1.745E-09	6.993E-10	-6.119E-10	-4.326E-10	1.631E-10	1.317E-10	-2.514E-11
Fe^{9+*}	20.	2.0E+04	2.237E-09	8.855E-10	-7.341E-10	-4.306E-10	2.561E-10	1.225E-10	-6.323E-11

Table VII. Theoretical Electron-Impact Ionization Rate Coefficients for $e^- + Fe^{q+} \rightarrow Fe^{(q+1)+} + 2e^-$

Maxwellian Rate Coefficients (cm^3/s)

e^- Temp. (eV)	Fe^{10+}	Fe^{10+*}	Fe^{11+}	Fe^{11+*}	Fe^{12+}	Fe^{13+}
1.0E+00	0.00E+00	0.00E+00	0.00E+00	0.00E+00	0.00E+00	0.00E+00
2.0E+00	0.00E+00	0.00E+00	0.00E+00	0.00E+00	0.00E+00	0.00E+00
4.0E+00	0.00E+00	1.61E-36	0.00E+00	1.56E-39	0.00E+00	0.00E+00
7.0E+00	9.29E-29	4.46E-25	4.14E-31	9.10E-27	1.74E-33	3.20E-35
1.0E+01	4.80E-23	1.81E-20	9.02E-25	1.18E-21	1.80E-26	8.38E-28
2.0E+01	2.41E-16	4.68E-15	2.51E-17	1.09E-15	3.02E-18	4.60E-19
4.0E+01	6.08E-13	2.68E-12	1.56E-13	1.10E-12	4.53E-14	1.35E-14
7.0E+01	1.89E-11	4.55E-11	7.28E-12	2.35E-11	3.07E-12	1.26E-12
1.0E+02	7.71E-11	1.48E-10	3.55E-11	8.43E-11	1.76E-11	8.49E-12
2.0E+02	4.30E-10	6.37E-10	2.50E-10	4.13E-10	1.56E-10	9.55E-11
4.0E+02	1.06E-09	1.38E-09	6.94E-10	9.73E-10	5.00E-10	3.42E-10
7.0E+02	1.50E-09	1.86E-09	1.02E-09	1.36E-09	7.91E-10	5.58E-10
1.0E+03	1.67E-09	2.02E-09	1.14E-09	1.51E-09	9.12E-10	6.48E-10
2.0E+03	1.70E-09	2.02E-09	1.17E-09	1.53E-09	9.71E-10	6.91E-10
4.0E+03	1.50E-09	1.76E-09	1.03E-09	1.34E-09	8.71E-10	6.19E-10
7.0E+03	1.27E-09	1.49E-09	8.68E-10	1.14E-09	7.44E-10	5.25E-10
1.0E+04	1.12E-09	1.31E-09	7.46E-10	1.01E-09	6.59E-10	4.52E-10
2.0E+04	8.49E-10	9.91E-10	4.79E-10	7.60E-10	5.00E-10	2.91E-10

Chebychev Fitting Parameters for Rate Coefficients

	E_{min} (eV)	E_{max} (eV)	A0	A1	A2	A3	A4	A5	A6
Fe^{10+}	20.	2.0E+04	1.485E-09	6.625E-10	-4.442E-10	-3.924E-10	1.120E-10	1.630E-10	2.290E-11
Fe^{10+*}	20.	2.0E+04	1.818E-09	7.684E-10	-5.605E-10	-4.070E-10	1.701E-10	1.395E-10	-1.753E-11
Fe^{11+}	40.	2.0E+04	1.084E-09	3.960E-10	-3.852E-10	-1.865E-10	1.177E-10	3.063E-11	-3.411E-11
Fe^{11+*}	20.	2.0E+04	1.348E-09	5.919E-10	-4.041E-10	-3.356E-10	1.082E-10	1.301E-10	8.421E-12
Fe^{12+}	40.	2.0E+04	9.013E-10	3.689E-10	-2.757E-10	-1.670E-10	9.029E-11	4.974E-11	-1.353E-11
Fe^{13+}	40.	2.0E+04	6.116E-10	2.444E-10	-2.089E-10	-1.382E-10	5.599E-11	4.054E-11	-6.163E-12

Table VIII. Theoretical Electron-Impact Ionization Rate Coefficients for $e^- + Fe^{q+} \rightarrow Fe^{(q+1)+} + 2e^-$

Maxwellian Rate Coefficients (cm^3/s)

e^- Temp. (eV)	Fe^{14+}	Fe^{14+*}	Fe^{15+}	Fe^{15+} (RRDA)
1.0E+00	0.00E+00	0.00E+00	0.00E+00	0.00E+00
2.0E+00	0.00E+00	0.00E+00	0.00E+00	0.00E+00
4.0E+00	0.00E+00	0.00E+00	0.00E+00	0.00E+00
7.0E+00	7.25E-39	2.76E-37	0.00E+00	0.00E+00
1.0E+01	2.48E-30	3.08E-29	8.73E-33	2.80E-32
2.0E+01	2.37E-20	8.10E-20	9.92E-22	1.61E-21
4.0E+01	2.56E-15	4.63E-15	3.49E-16	4.34E-16
7.0E+01	4.27E-13	5.70E-13	1.07E-13	1.37E-13
1.0E+02	3.83E-12	4.41E-12	1.32E-12	1.73E-12
2.0E+02	6.36E-11	6.25E-11	3.04E-11	3.75E-11
4.0E+02	2.79E-10	2.67E-10	1.51E-10	1.70E-10
7.0E+02	5.00E-10	4.88E-10	2.87E-10	3.06E-10
1.0E+03	6.05E-10	5.98E-10	3.58E-10	3.77E-10
2.0E+03	6.81E-10	6.89E-10	4.21E-10	4.33E-10
4.0E+03	6.28E-10	6.43E-10	3.97E-10	4.05E-10
7.0E+03	5.42E-10	5.59E-10	3.47E-10	3.52E-10
1.0E+04	4.82E-10	4.98E-10	3.10E-10	3.14E-10
2.0E+04	3.68E-10	3.81E-10	2.37E-10	2.40E-10

Chebychev Fitting Parameters for Rate Coefficients

	E_{min} (eV)	E_{max} (eV)	A0	A1	A2	A3	A4	A5	A6
Fe^{14+}	70.	2.0E+04	6.763E-10	2.605E-10	-2.034E-10	-8.340E-11	7.304E-11	6.434E-12	-2.382E-11
Fe^{14+*}	70.	2.0E+04	6.844E-10	2.694E-10	-1.996E-10	-8.971E-11	6.880E-11	1.050E-11	-2.062E-11
Fe^{15+}	70.	2.0E+04	4.155E-10	1.695E-10	-1.180E-10	-5.964E-11	4.104E-11	8.717E-12	-1.214E-11
Fe^{15+} (RRDA)	70.	2.0E+04	4.311E-10	1.706E-10	-1.256E-10	-5.630E-11	4.405E-11	5.736E-12	-1.375E-11

Table IX. Theoretical Electron-Impact Ionization Rate Coefficients for $e^- + Fe^{q+} \rightarrow Fe^{(q+1)+} + 2e^-$

Maxwellian Rate Coefficients (cm^3/s)

e^- Temp. (eV)	Fe^{16+}	Fe^{17+}	Fe^{18+}	Fe^{19+}	Fe^{20+}
7.0E+01	4.70E-19	8.67E-20	1.57E-20	2.34E-21	3.76E-22
1.0E+02	1.78E-16	5.00E-17	1.39E-17	3.22E-18	8.12E-19
2.0E+02	1.88E-13	8.65E-14	3.96E-14	1.58E-14	6.67E-15
4.0E+02	6.38E-12	3.78E-12	2.22E-12	1.18E-12	6.47E-13
7.0E+02	2.95E-11	1.96E-11	1.29E-11	7.77E-12	4.76E-12
1.0E+03	5.45E-11	3.79E-11	2.61E-11	1.66E-11	1.07E-11
2.0E+03	1.10E-10	8.08E-11	5.88E-11	4.02E-11	2.73E-11
3.0E+03	1.36E-10	1.02E-10	7.57E-11	5.30E-11	3.68E-11
4.0E+03	1.48E-10	1.13E-10	8.48E-11	6.03E-11	4.23E-11
5.0E+03	1.55E-10	1.19E-10	9.00E-11	6.46E-11	4.58E-11
6.0E+03	1.58E-10	1.22E-10	9.28E-11	6.70E-11	4.78E-11
7.0E+03	1.59E-10	1.23E-10	9.40E-11	6.82E-11	4.87E-11
8.0E+03	1.59E-10	1.23E-10	9.47E-11	6.90E-11	4.94E-11
9.0E+03	1.58E-10	1.23E-10	9.47E-11	6.91E-11	4.96E-11
1.0E+04	1.57E-10	1.23E-10	9.44E-11	6.91E-11	4.97E-11
1.2E+04	1.54E-10	1.20E-10	9.30E-11	6.81E-11	4.91E-11
1.5E+04	1.49E-10	1.17E-10	9.04E-11	6.64E-11	4.80E-11
2.0E+04	1.40E-10	1.10E-10	8.56E-11	6.35E-11	4.62E-11

Chebychev Fitting Parameters for Rate Coefficients

	E_{min} (eV)	E_{max} (eV)	A0	A1	A2	A3	A4	A5	A6
Fe^{16+}	200.	2.E+04.	1.712/9E-10	8.82601E-11	-1.81630E-11	-2.16876E-11	4.10843E-12	3.13239E-12	-1.69224E-12
Fe^{17+}	200.	2.E+04.	1.30837E-10	6.95299E-11	-1.16036E-11	-1.73318E-11	2.41865E-12	2.79580E-12	-1.15335E-12
Fe^{18+}	200.	2.E+04.	9.88938E-11	5.39741E-11	-7.14323E-12	-1.35460E-11	1.28830E-12	2.37495E-12	-7.49385E-13
Fe^{19+}	200.	2.E+04.	7.08654E-11	3.98340E-11	-3.73340E-12	-9.98940E-12	4.32819E-13	1.90022E-12	-3.71562E-13
Fe^{20+}	200.	2.E+04.	5.02092E-11	2.88631E-11	-1.84257E-12	-7.18531E-12	1.99540E-14	1.43894E-12	-1.58607E-13

Table X. Theoretical Electron-Impact Ionization Rate Coefficients for $e^- + Fe^{q+} \rightarrow Fe^{(q+1)+} + 2e^-$

Maxwellian Rate Coefficients (cm^3/s)

e^- Temp. (eV)	Fe^{21+}	Fe^{22+}	Fe^{23+}	Fe^{24+}	Fe^{25+}
7.0E+01	5.27E-23	2.68E-24	2.84E-25	0.00E+00	0.00E+00
1.0E+02	1.76E-19	1.93E-20	3.20E-21	0.00E+00	0.00E+00
2.0E+02	2.65E-15	6.29E-16	1.75E-16	9.08E-32	4.58E-33
4.0E+02	3.13E-13	1.20E-13	4.29E-14	3.39E-22	5.23E-23
7.0E+02	2.61E-12	1.18E-12	4.71E-13	4.73E-18	1.17E-18
1.0E+03	6.18E-12	2.98E-12	1.25E-12	2.26E-16	6.70E-17
2.0E+03	1.69E-11	8.82E-12	3.93E-12	2.23E-14	8.24E-15
3.0E+03	2.33E-11	1.25E-11	5.79E-12	1.04E-13	4.12E-14
4.0E+03	2.71E-11	1.49E-11	7.06E-12	2.42E-13	9.97E-14
5.0E+03	2.97E-11	1.65E-11	7.99E-12	3.96E-13	1.67E-13
6.0E+03	3.12E-11	1.74E-11	8.62E-12	5.51E-13	2.36E-13
7.0E+03	3.19E-11	1.79E-11	9.01E-12	6.97E-13	3.02E-13
8.0E+03	3.25E-11	1.84E-11	9.38E-12	8.33E-13	3.64E-13
9.0E+03	3.27E-11	1.85E-11	9.60E-12	9.58E-13	4.21E-13
1.0E+04	3.29E-11	1.87E-11	9.80E-12	1.07E-12	4.74E-13
1.2E+04	3.25E-11	1.85E-11	9.93E-12	1.27E-12	5.64E-13
1.5E+04	3.18E-11	1.82E-11	1.00E-11	1.49E-12	6.70E-13
2.0E+04	3.10E-11	1.80E-11	1.02E-11	1.72E-12	7.81E-13

Chebychev Fitting Parameters for Rate Coefficients

	E_{min} (eV)	E_{max} (eV)	A0	A1	A2	A3	A4	A5	A6
Fe^{21+}	200.	2.E+04	3.26206E-11	1.92107E-11	-5.96805E-13	-4.70444E-12	-2.02019E-13	9.84203E-13	-1.85937E-14
Fe^{22+}	200.	2.E+04	1.82182E-11	1.10297E-11	7.41865E-14	-2.62089E-12	-2.53155E-13	5.72536E-13	5.18376E-14
Fe^{23+}	200.	2.E+04	9.39620E-12	5.98496E-12	5.65971E-13	-1.12187E-12	-2.08927E-13	2.25523E-13	3.36430E-14
Fe^{24+}	1000	2.E+04	1.26599E-12	8.98312E-13	2.73254E-13	-4.12907E-14	-4.57171E-14	3.28509E-15	0.00000E+00
Fe^{25+}	1000	2.E+04	5.64060E-13	4.04743E-13	1.29701E-13	-1.50931E-14	-2.12768E-14	7.36451E-16	0.00000E+00

Table XI. Experimental Electron-Impact Ionization Rate Coefficients for $e^- + Fe^{q+} \rightarrow Fe^{(q+1)+} + 2e^-$

Maxwellian Rate Coefficients (cm^3/s)

e^- Temp. (eV)	Fe^+	Fe^{2+}	Fe^{5+}	Fe^{6+}	Fe^{9+}	Fe^{11+}	Fe^{13+}	Fe^{15+}
1.0E+00	2.64E-15	3.71E-20	0.00E+00	0.00E+00	0.00E+00	0.00E+00	0.00E+00	0.00E+00
2.0E+00	7.77E-12	1.63E-14	4.99E-30	2.76E-36	0.00E+00	0.00E+00	0.00E+00	0.00E+00
4.0E+00	5.29E-10	1.27E-11	2.10E-19	1.37E-22	3.71E-33	0.00E+00	0.00E+00	0.00E+00
7.0E+00	3.53E-09	2.70E-10	8.12E-15	1.10E-16	4.49E-23	1.36E-30	9.27E-36	0.00E+00
1.0E+01	7.83E-09	1.02E-09	5.76E-13	2.63E-14	4.78E-19	2.62E-24	6.02E-28	4.11E-36
2.0E+01	2.14E-08	5.84E-09	8.94E-11	1.64E-11	2.51E-14	5.52E-17	7.91E-19	3.03E-23
4.0E+01	3.83E-08	1.66E-08	1.21E-09	4.33E-10	6.95E-12	2.63E-13	2.57E-14	8.58E-17
7.0E+01	5.14E-08	2.86E-08	3.88E-09	1.84E-09	9.02E-11	1.07E-11	2.09E-12	6.87E-14
1.0E+02	5.85E-08	3.68E-08	6.33E-09	3.34E-09	2.66E-10	4.93E-11	1.28E-11	1.14E-12
2.0E+02	6.81E-08	5.13E-08	1.15E-08	6.91E-09	1.02E-09	3.26E-10	1.31E-10	3.21E-11
4.0E+02	7.00E-08	6.14E-08	1.55E-08	1.00E-08	2.05E-09	8.78E-10	4.64E-10	1.63E-10
7.0E+02	6.60E-08	6.48E-08	1.69E-08	1.13E-08	2.66E-09	1.30E-09	7.95E-10	3.22E-10
1.0E+03	6.16E-08	6.42E-08	1.68E-08	1.15E-08	2.84E-09	1.47E-09	9.72E-10	4.25E-10
2.0E+03	5.12E-08	5.81E-08	1.53E-08	1.06E-08	2.78E-09	1.60E-09	1.17E-09	5.90E-10
4.0E+03	4.08E-08	4.85E-08	1.28E-08	8.91E-09	2.40E-09	1.52E-09	1.17E-09	6.78E-10
7.0E+03	3.32E-08	4.02E-08	1.06E-08	7.41E-09	2.01E-09	1.37E-09	1.07E-09	6.84E-10
1.0E+04	2.89E-08	3.52E-08	9.29E-09	6.50E-09	1.77E-09	1.25E-09	9.78E-10	6.60E-10
2.0E+04	2.16E-08	2.64E-08	6.95E-09	4.88E-09	1.32E-09	9.94E-10	7.79E-10	5.73E-10

Chebychev Fitting Parameters for Rate Coefficients

	E_{min} (eV)	E_{max} (eV)	A0	A1	A2	A3	A4	A5	A6
Fe^+	2.0	2.0E+04	6.007E-08	1.673E-08	-2.637E-08	-6.450E-09	9.454E-09	4.599E-10	-2.370E-09
Fe^{2+}	4.0	2.0E+04	5.775E-08	2.105E-08	-2.058E-08	-1.014E-08	5.751E-09	2.379E-09	-7.403E-10
Fe^{5+}	10.	2.0E+04	1.525E-08	5.373E-09	-5.550E-09	-2.259E-09	2.009E-09	3.587E-10	-6.116E-10
Fe^{6+}	20.	2.0E+04	1.099E-08	3.395E-09	-4.039E-09	-9.455E-10	1.321E-09	-2.043E-11	-3.310E-10
Fe^{9+}	40.	2.0E+04	2.820E-09	9.086E-10	-9.802E-10	-2.458E-10	3.275E-10	-5.870E-12	-9.335E-11
Fe^{11+}	40.	2.0E+04	1.631E-09	6.962E-10	-4.154E-10	-2.401E-10	1.353E-10	4.167E-11	-3.710E-11
Fe^{13+}	40.	2.0E+04	1.152E-09	5.537E-10	-2.479E-10	-2.367E-10	5.888E-11	7.606E-11	5.931E-12
Fe^{15+}	70.	2.0E+04	7.206E-10	3.761E-10	-8.551E-11	-1.033E-10	1.846E-11	1.340E-11	-6.911E-12

Table XII. Sample BASIC Program to Calculate Rate Coefficients from Chebyshev Fitting Parameters.

```
10      REM   PROGRAM CHEBFE
20      REM CHBFIT PROGRAM IS A BASIC PROGRAM DERIVED FROM A PROGRAM IN
30      REM "ELEMENTARY NUMERICAL ANALYSIS: AN ALGORITHMIC APPROACH",S.D. CONTE
40      REM AND C. DE BOOR, MCGRAW-HILL, INC., P 254, 1972.
50      DIM D(7)
60      NTERMS=7
70      INPUT"ENTER Emin (eV)  ",EMIN:INPUT"ENTER Emax (eV)  ",EMAX
80      EMINL=LOG(EMIN)
90      EMAXL=LOG(EMAX)
100     PRINT USING "ENTER # COEFFICIENTS A0 THRU A6";NTERMS
110     FOR J=1 TO NTERMS
120     INPUT D(J):NEXT J
130     PRINT USING "INPUT ENERGY (eV) BETWEEN ###.# AND #.#^^^^ FOR THE RATE CO
EF. CALCULATION";EMIN;EMAX
140     REM  GET ENERGY FOR CALCULATION AND USE THREE TERM RECURRENCE RELATION
150     INPUT X
160     K=NTERMS
170     CHEB=D(K)
180     IF X<0 THEN END
190     X=LOG(X)
200     K=K-1
210     IF K=0 THEN END
220     XNORM=(X-EMINL-(EMAXL-X))/(EMAXL-EMINL)
230     TWOX=2*XNORM
240     PREV2=0
250     PREV=CHEB
260     IF K=1 GOTO 310
270     CHEB=D(K)+TWOX*PREV-PREV2
280     PREV2=PREV
290     K=K-1
300     GOTO 250
310     CHEB=.5*D(1)+XNORM*PREV-PREV2
320     PRINT USING "##.##^^^^ = RATE COEFFICIENT (CM3/S)";CHEB
330     GOTO 130
340     END
```

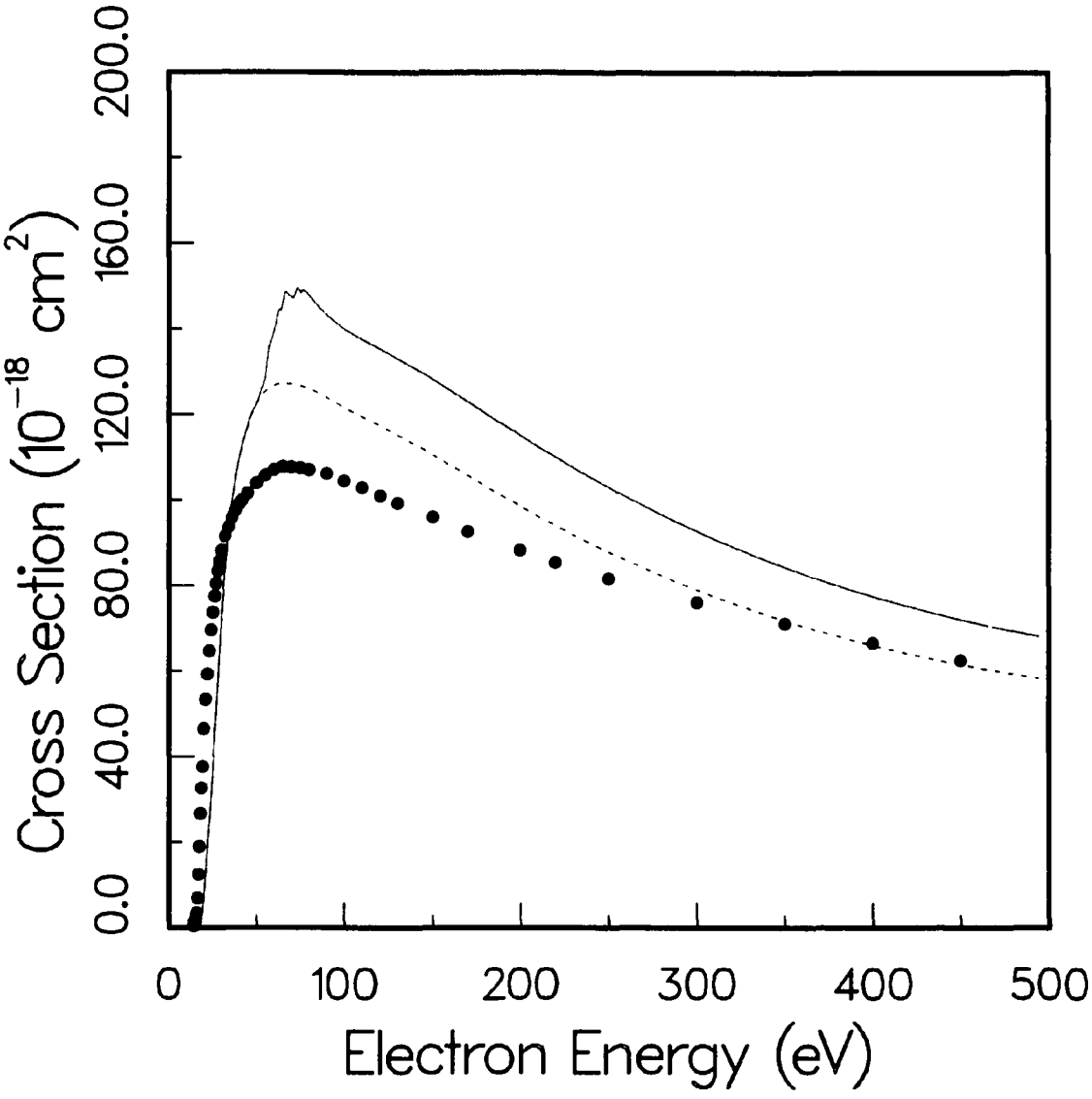

Fig. 1. Electron-impact ionization of Fe^+. Solid curve: total cross section from the $3p^6 3d^6 4s$ ground configuration in the average statistical model; dashed curve: direct cross section only; solid circles: experimental measurements (ref. 5).

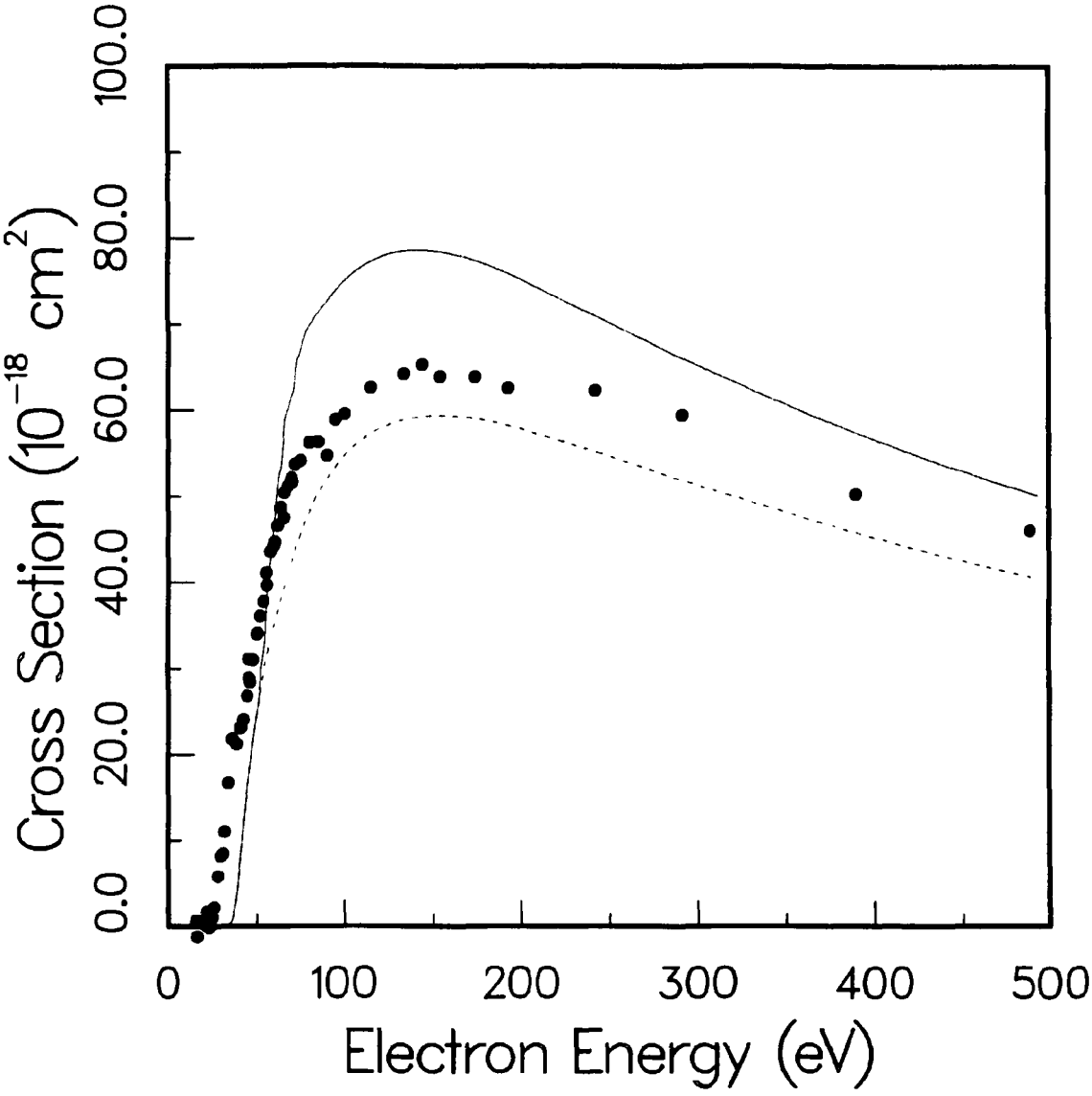

Fig. 2. Electron-impact ionization of Fe^{2+}. Solid curve: total cross section from the $3p^6 3d^6$ ground configuration in the average statistical model (ref. 18); dashed curve: direct cross section only; solid circles: experimental measurements (ref. 6).

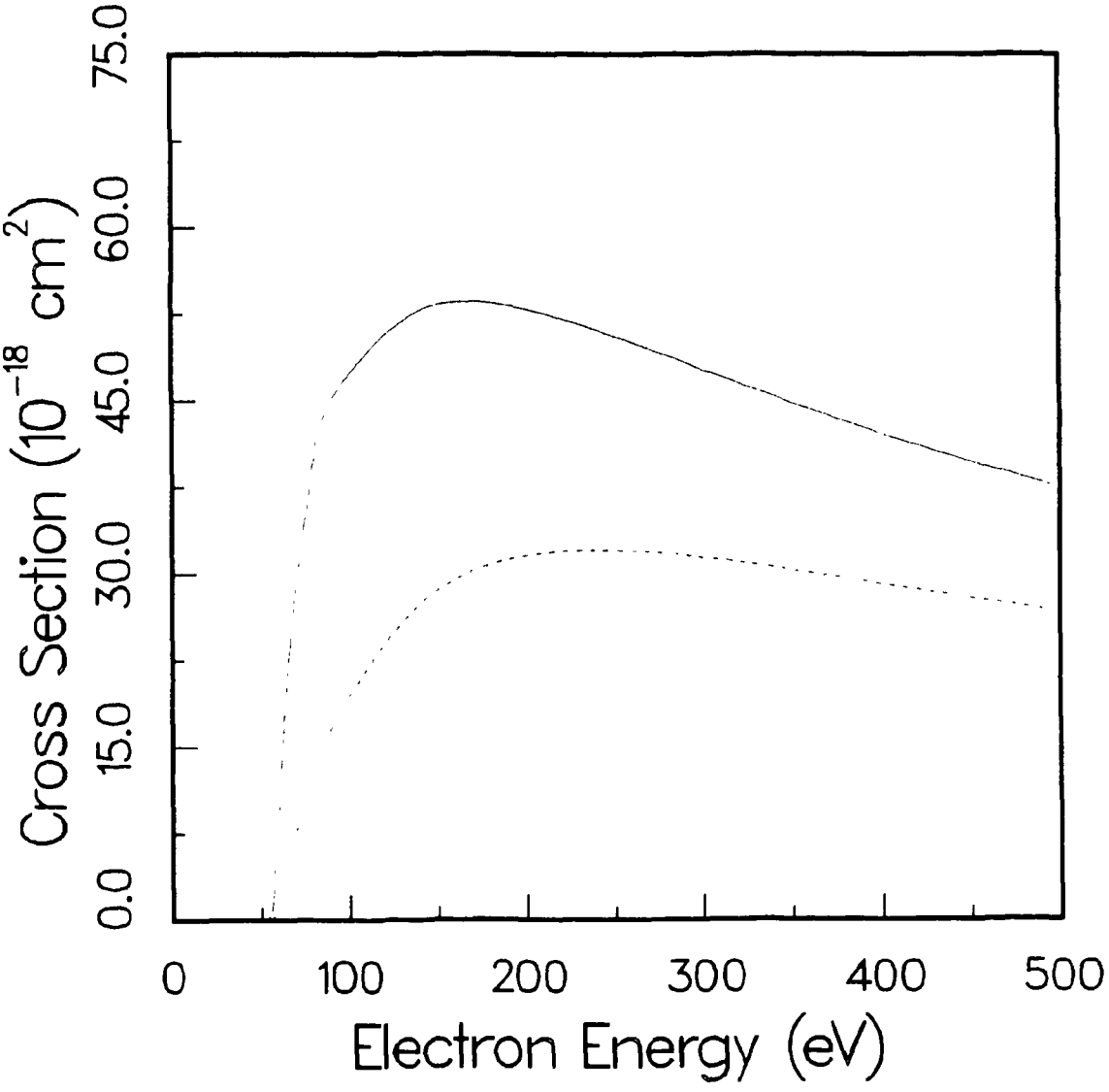

Fig. 3. Electron-impact ionization of Fe^{3+}. Solid curve: total cross section from the $3p^6 3d^5$ ground configuration in the average statistical model (ref. 18); dashed curve: direct cross section only.

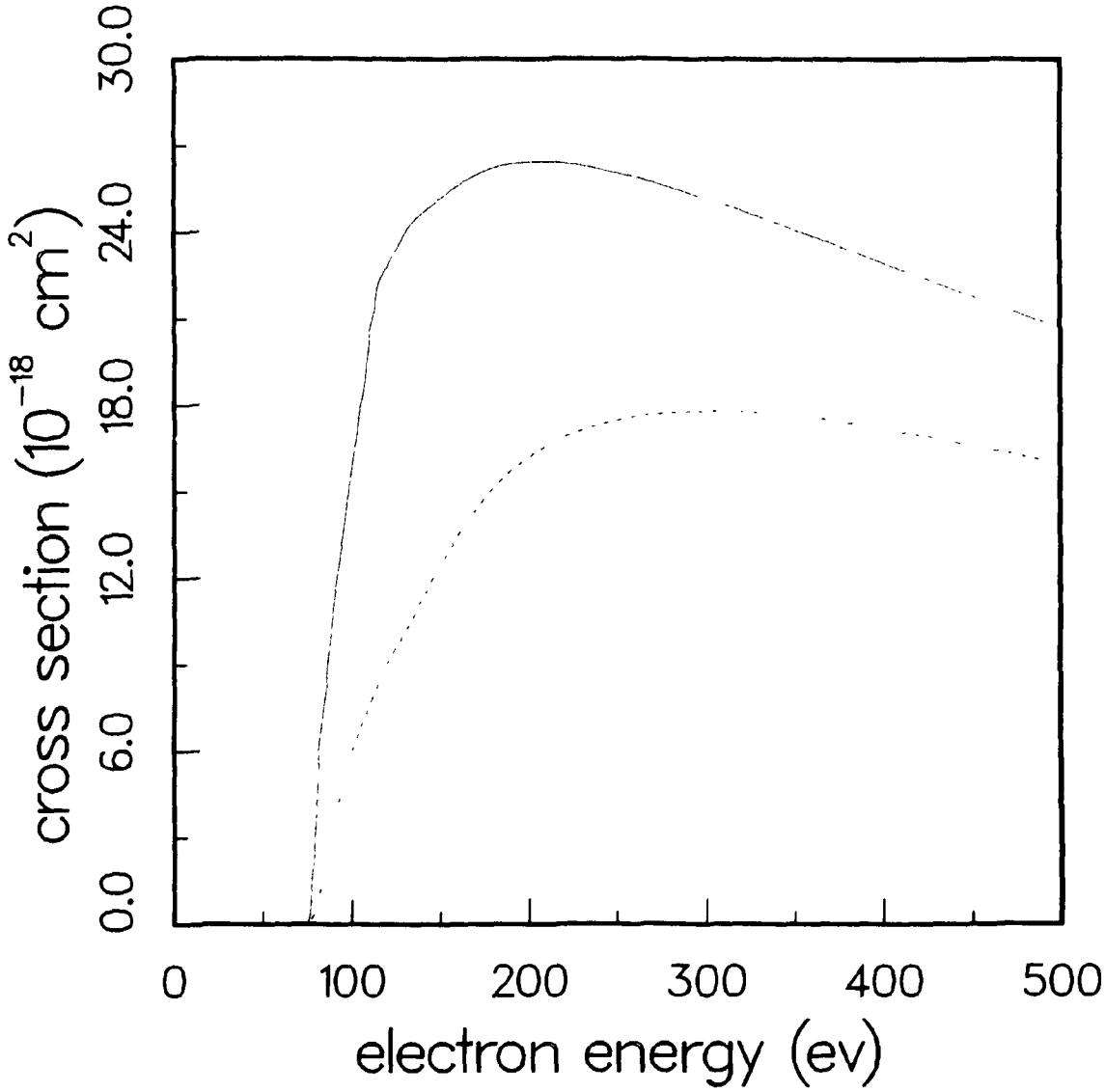

Fig. 4. Electron-impact ionization of Fe^{4+}. Solid curve: total cross section from the $3p^6 3d^4$ ground configuration in the average statistical model; dashed curve: direct cross section only.

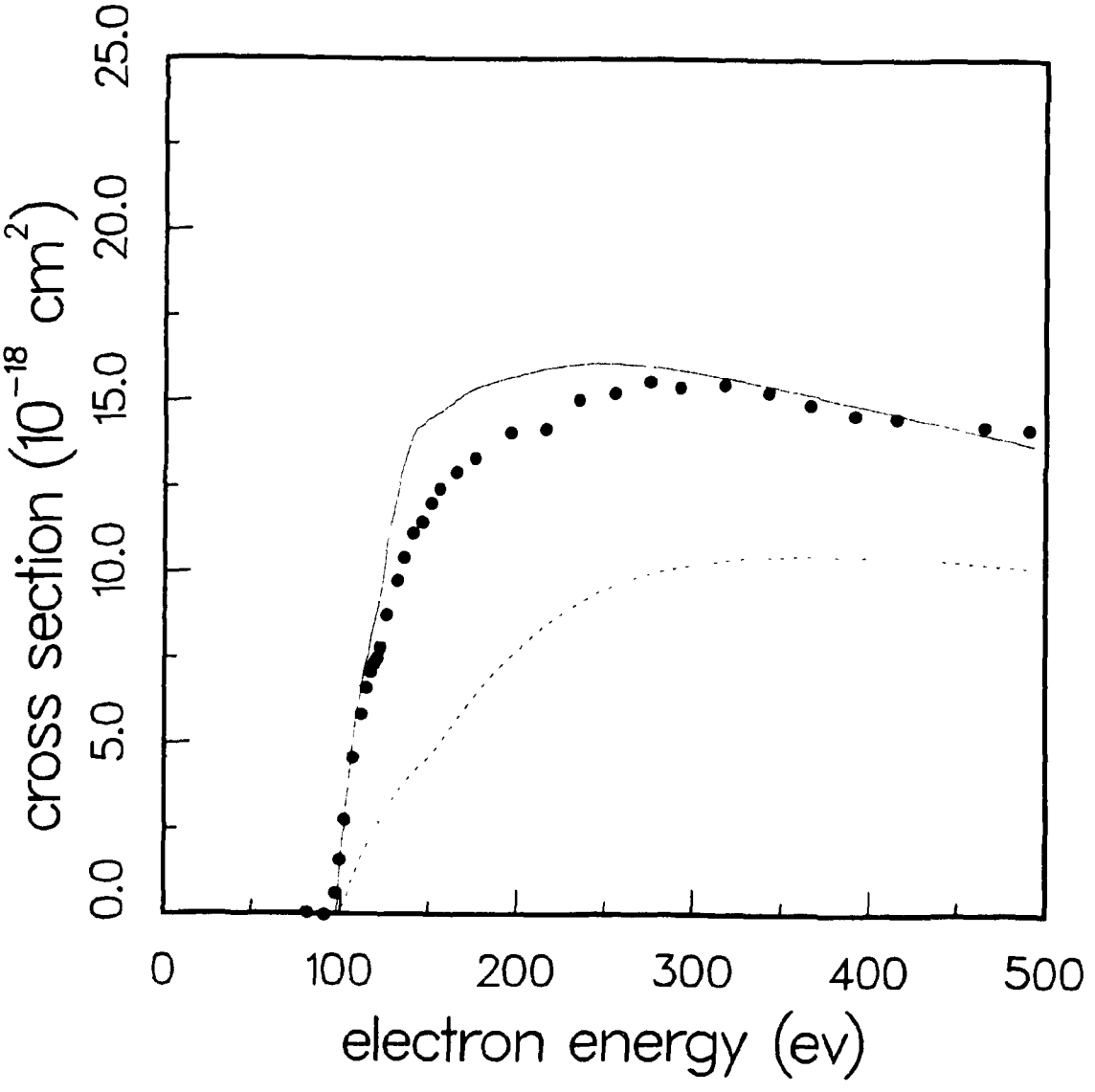

Fig. 5. Electron-impact ionization of Fe^{5+}. Solid curve: total cross section from the $3p^6 3d^3$ ground configuration in the average statistical model (ref. 19); dashed curve: direct cross section only; solid circles: experimental measurements (ref. 7).

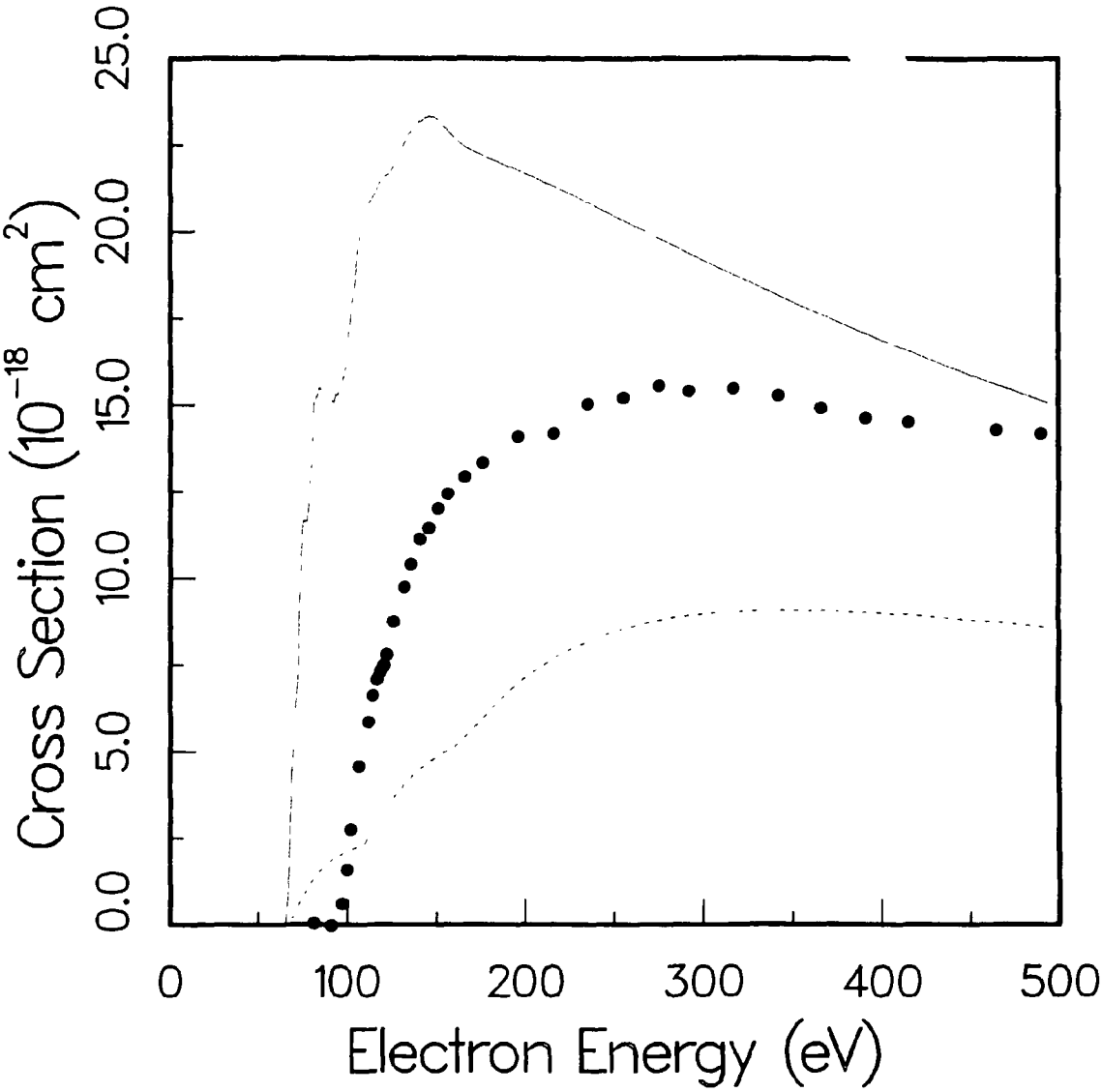

Fig. 6. Electron-impact ionization of Fe^{5+}. Solid curve: total cross section from the $3p^6 3d^2 4s$ excited configuration in the average statistical model (ref. 19); dashed curve: direct cross section only; solid circles: experimental measurements (ref. 7).

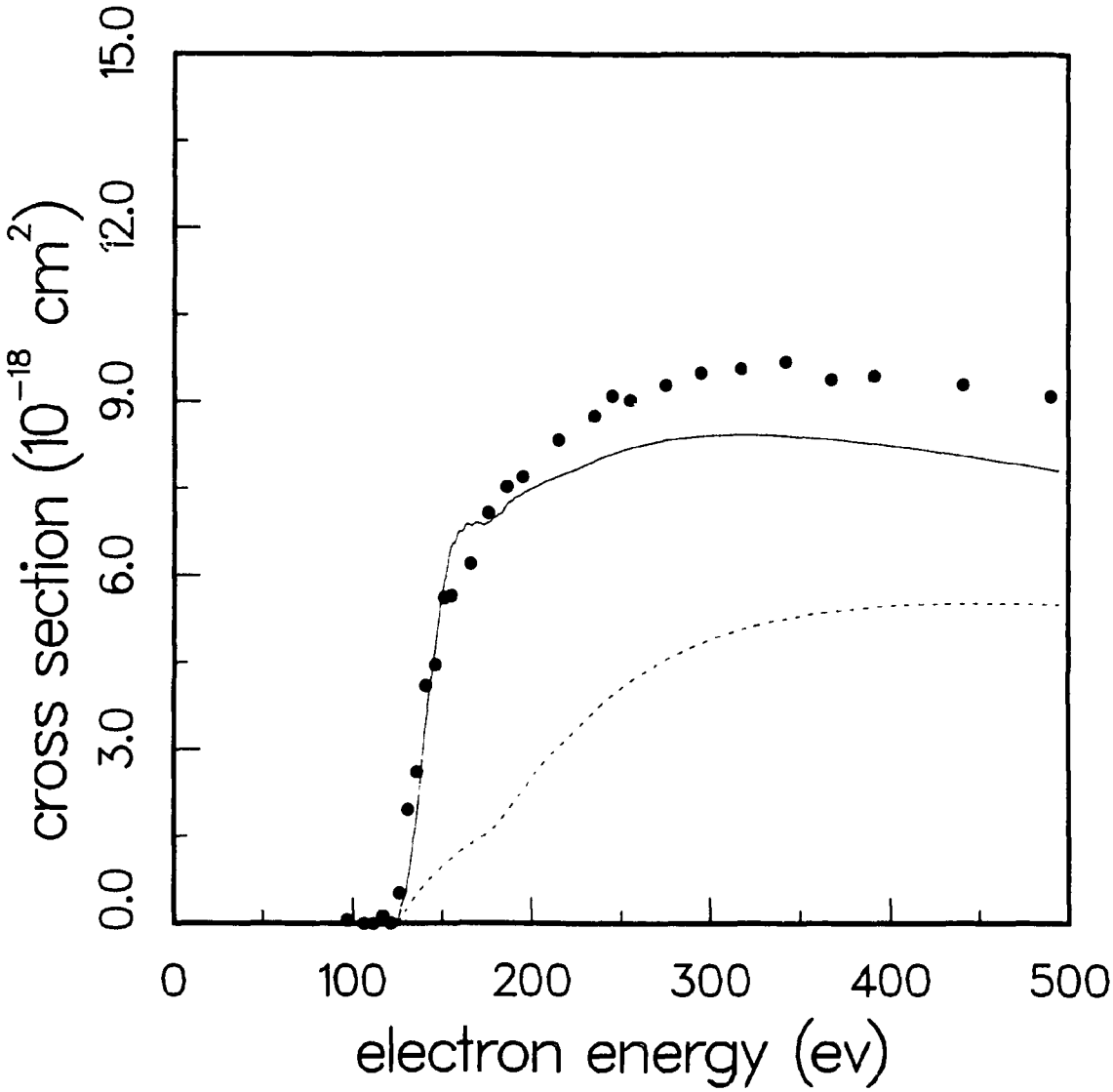

Fig. 7. Electron-impact ionization of Fe^{6+}. Solid curve: total cross section from the $3p^6 3d^2$ ground configuration in the average statistical model (ref. 19); dashed curve: direct cross section only; solid circles: experimental measurements (ref. 7).

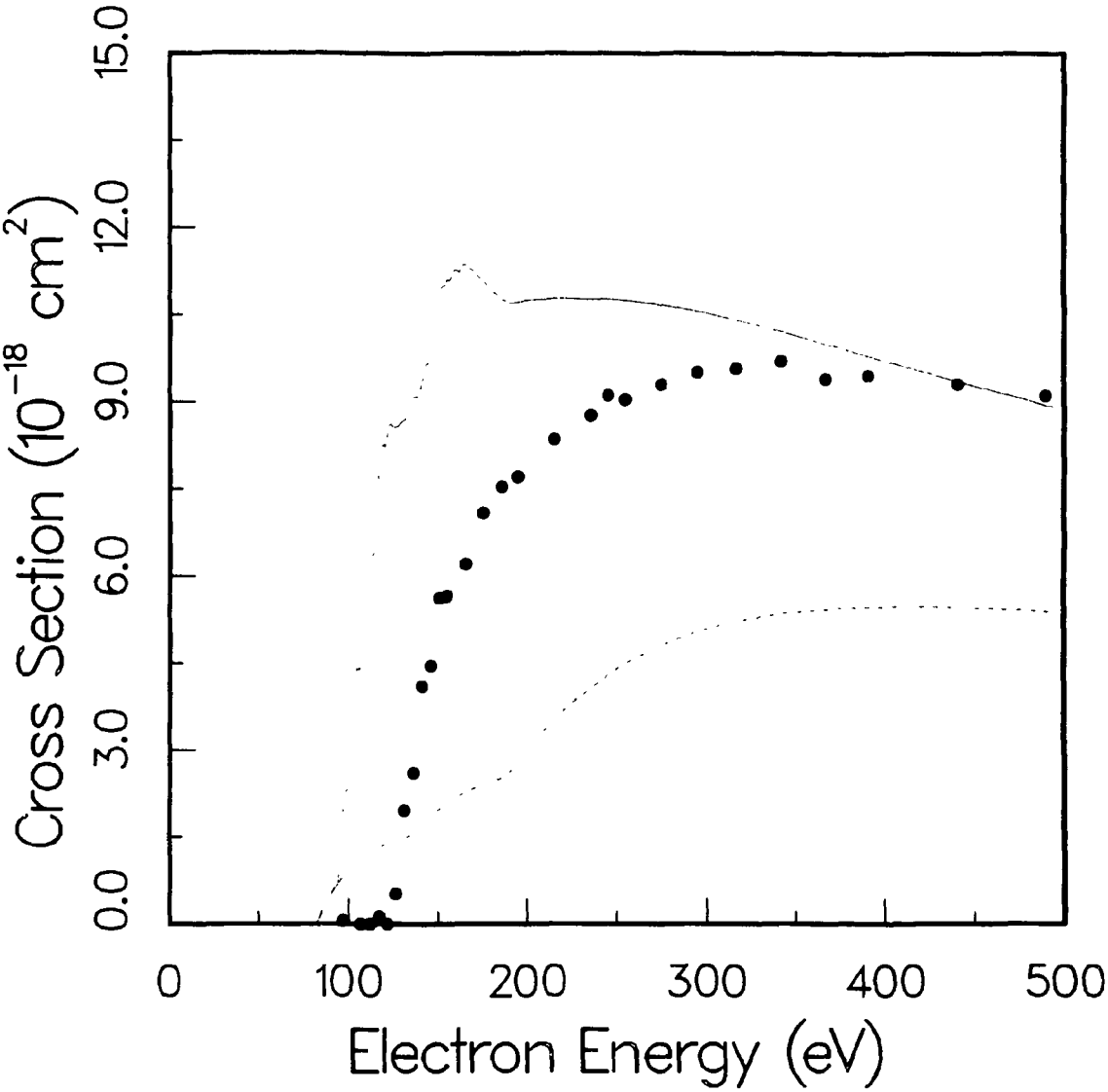

Fig. 8. Electron-impact ionization of Fe^{6+}. Solid curve: total cross section from the $3p^6 3d4s$ excited configuration in the average statistical model (ref. 19); dashed curve: direct cross section only; solid circles: experimental measurements (ref. 7).

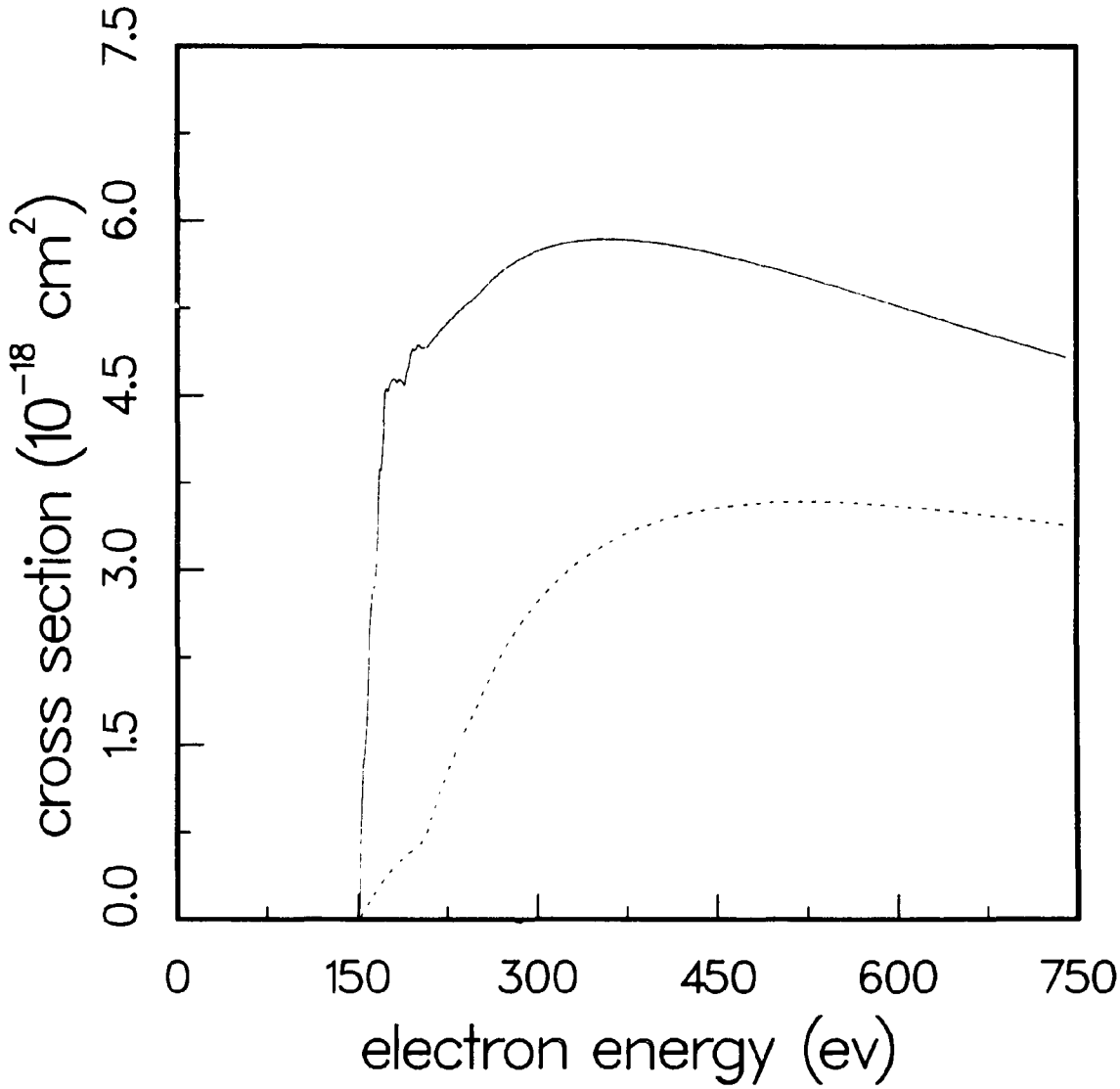

Fig. 9. Electron-impact ionization of Fe^{7+}. Solid curve: total cross section from the $3p^6 3d$ ground configuration in the average statistical model; dashed curve: direct cross section only.

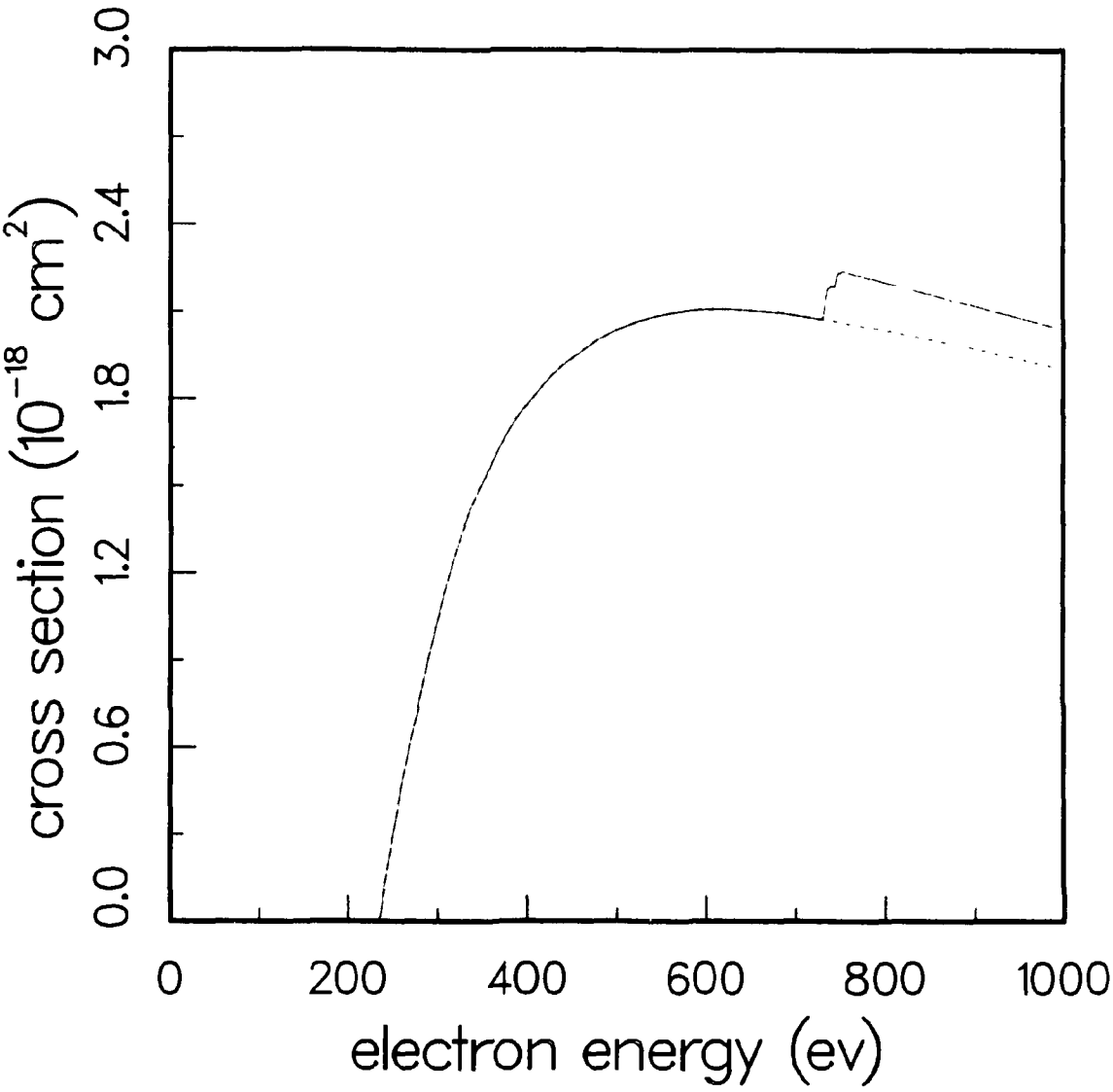

Fig. 10. Electron-impact ionization of Fe^{8+}. Solid curve: total cross section from the $3s^2 3p^6$ ground configuration in the average statistical model; dashed curve: direct cross section only.

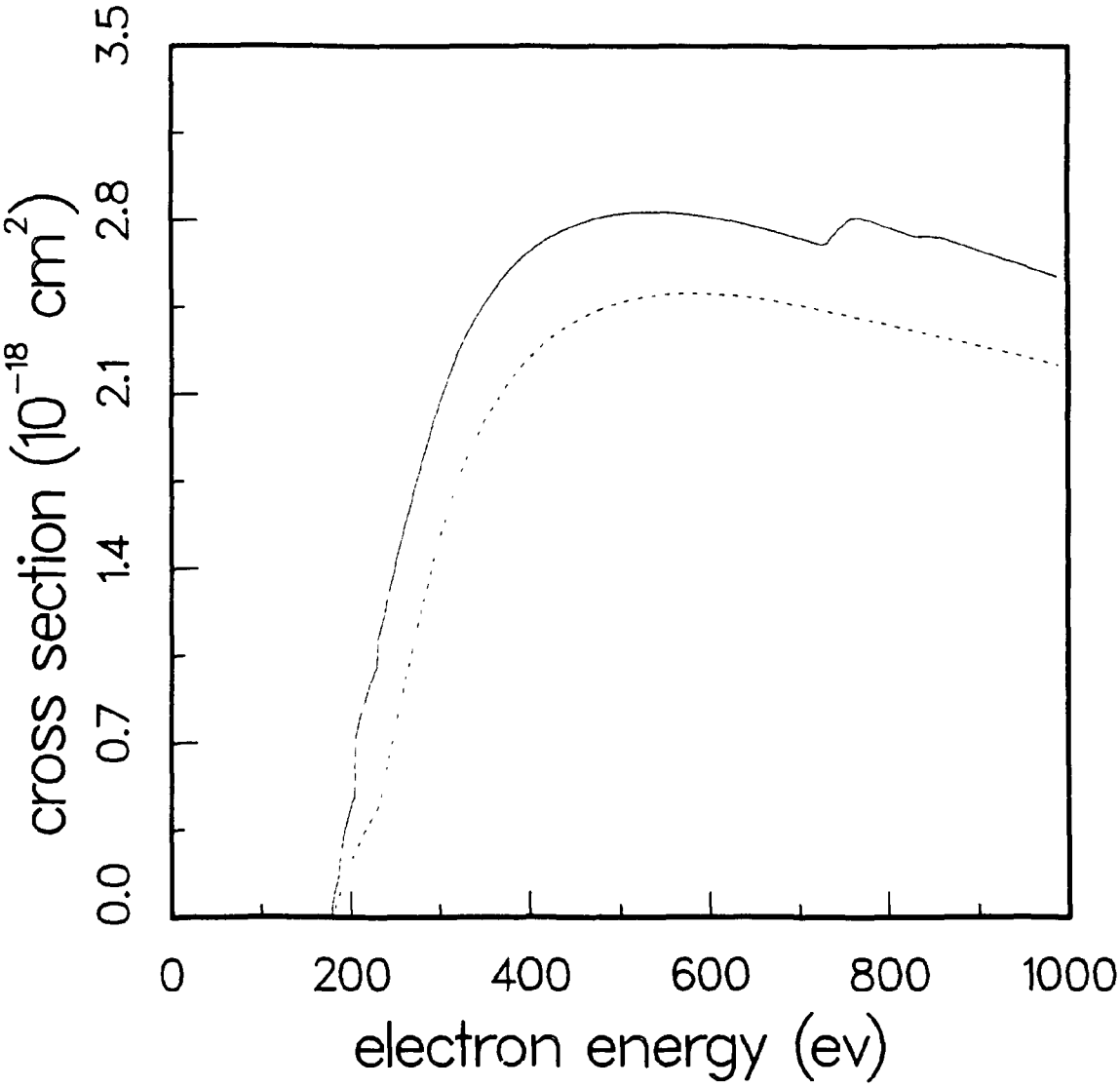

Fig. 11. Electron-impact ionization of Fe^{8+}. Solid curve: total cross section from the $3s^2 3p^5 3d$ excited configuration in the average statistical model; dashed curve: direct cross section only.

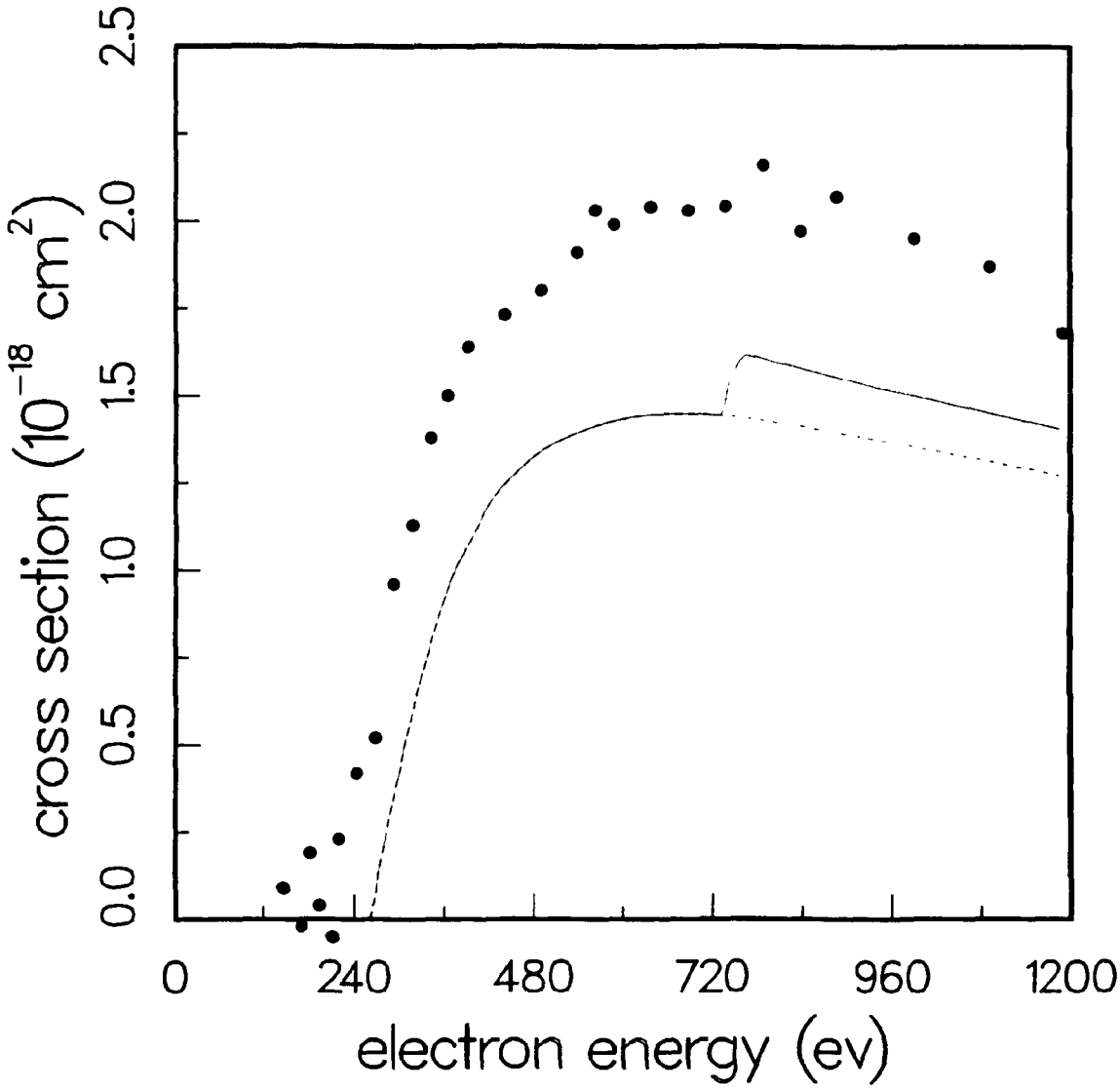

Fig. 12. Electron-impact ionization of Fe^{9+}. Solid curve: total cross section from the $3s^2 3p^5$ ground configuration in the average statistical model (ref. 19); dashed curve: direct cross section only; solid circles: experimental measurements (ref. 7).

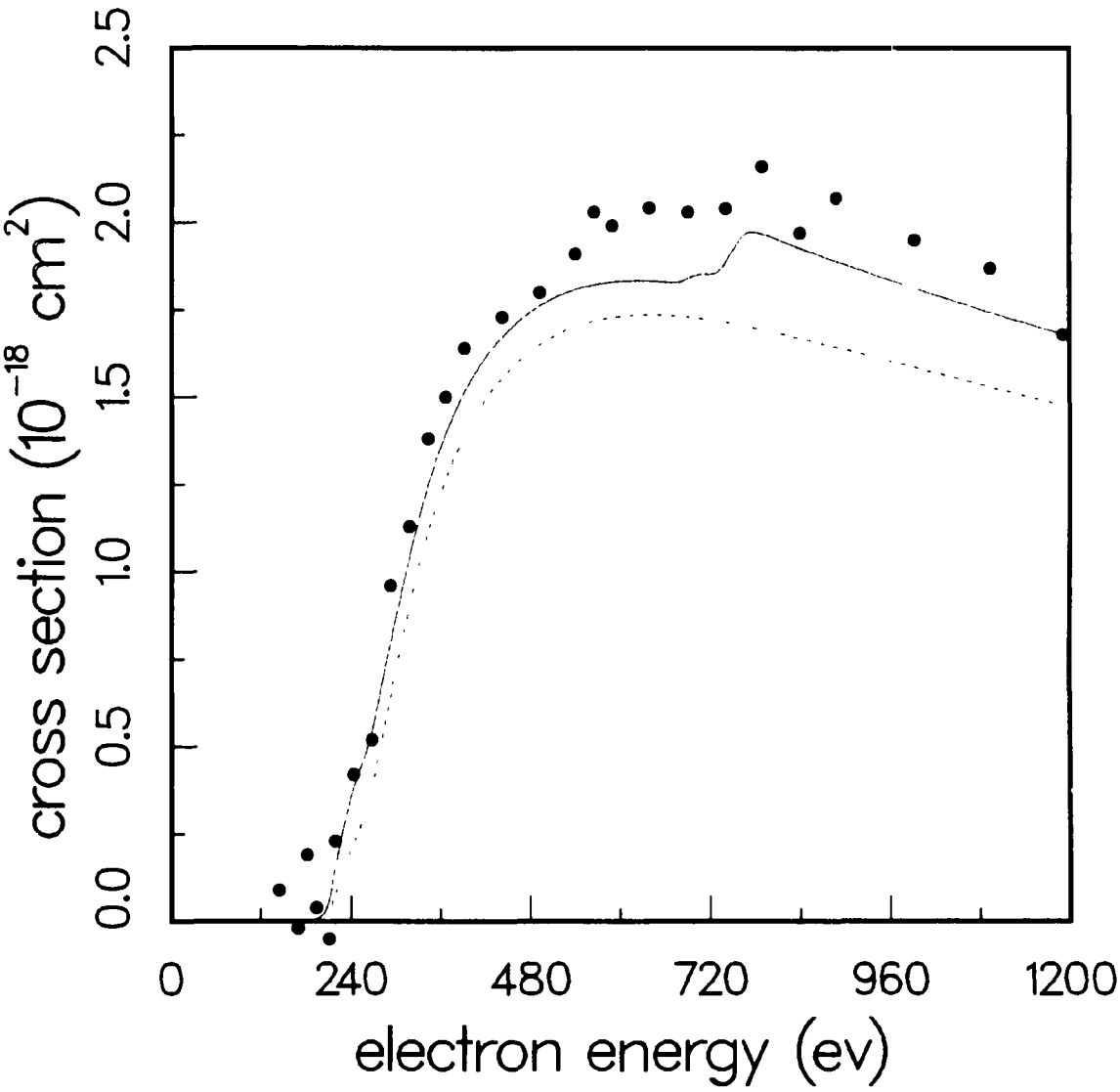

Fig. 13. Electron-impact ionization of Fe^{9+}. Solid curve: total cross section from the $3s^2 3p^4 3d$ excited configuration in the average statistical model (ref. 19); dashed curve: direct cross section only; solid circles: experimental measurements (ref. 7).

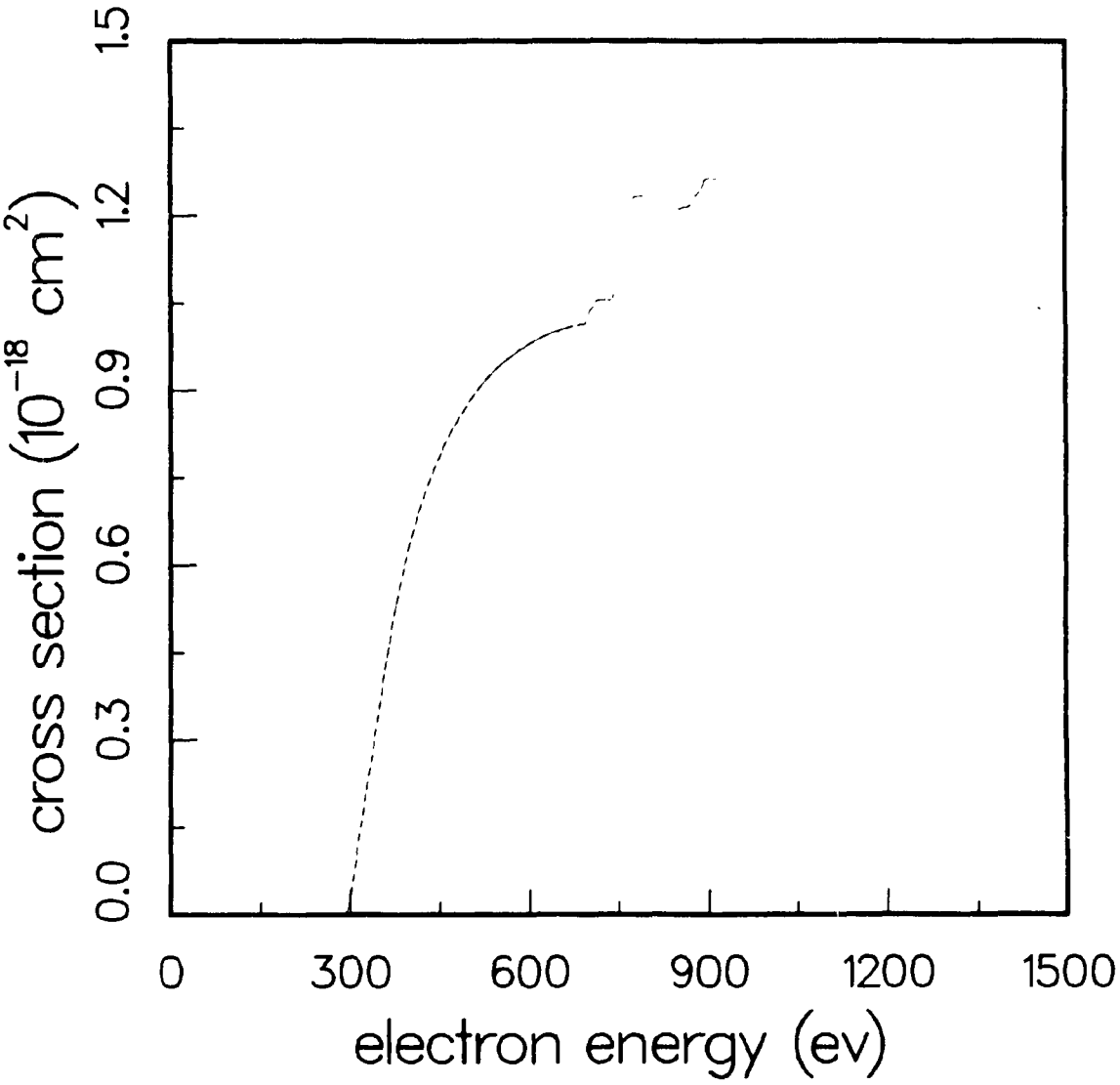

Fig. 14. Electron-impact ionization of Fe^{10+}. Solid curve: total cross section from the $3s^2 3p^4$ ground configuration in the average statistical model; dashed curve: direct cross section only.

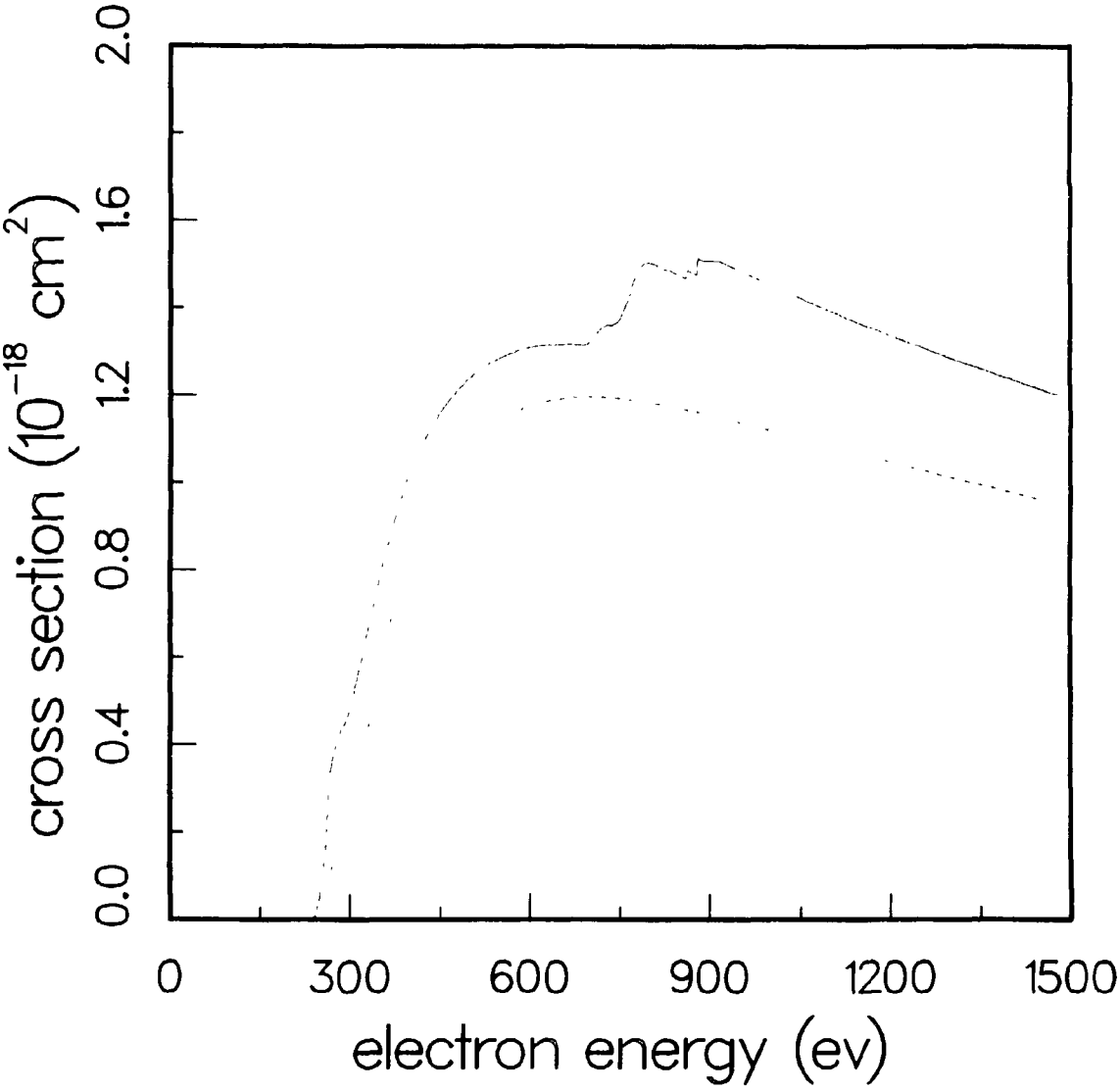

Fig. 15. Electron-impact ionization of Fe^{10+}. Solid curve: total cross section from the $3s^2 3p^3 3d$ excited configuration in the average statistical model; dashed curve: direct cross section only.

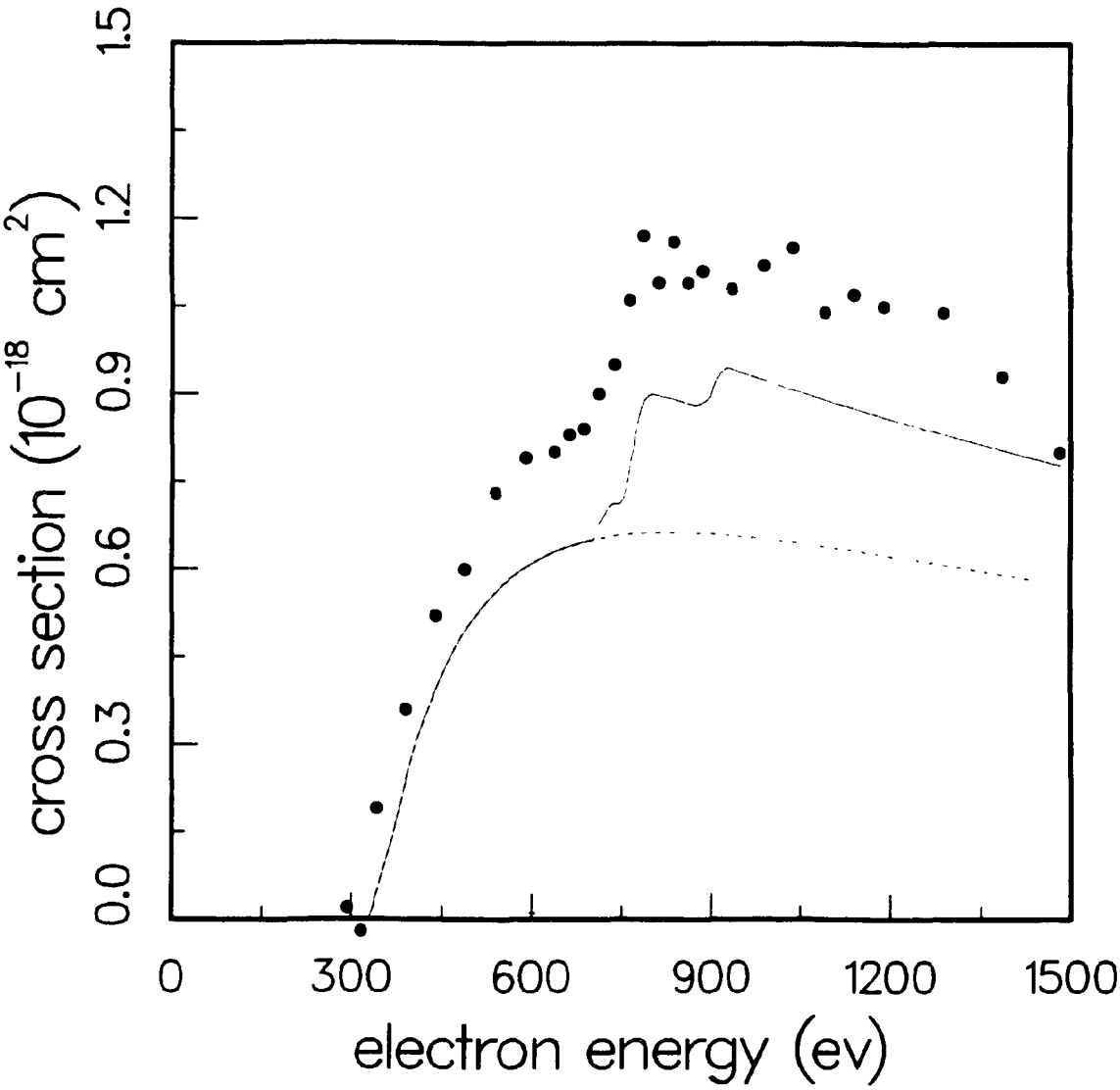

Fig. 16. Electron-impact ionization of Fe^{11+}. Solid curve: total cross section from the $3s^2 3p^3$ ground configuration in the average statistical model (ref. 19); dashed curve: direct cross section only; solid circles: experimental measurements (ref. 8).

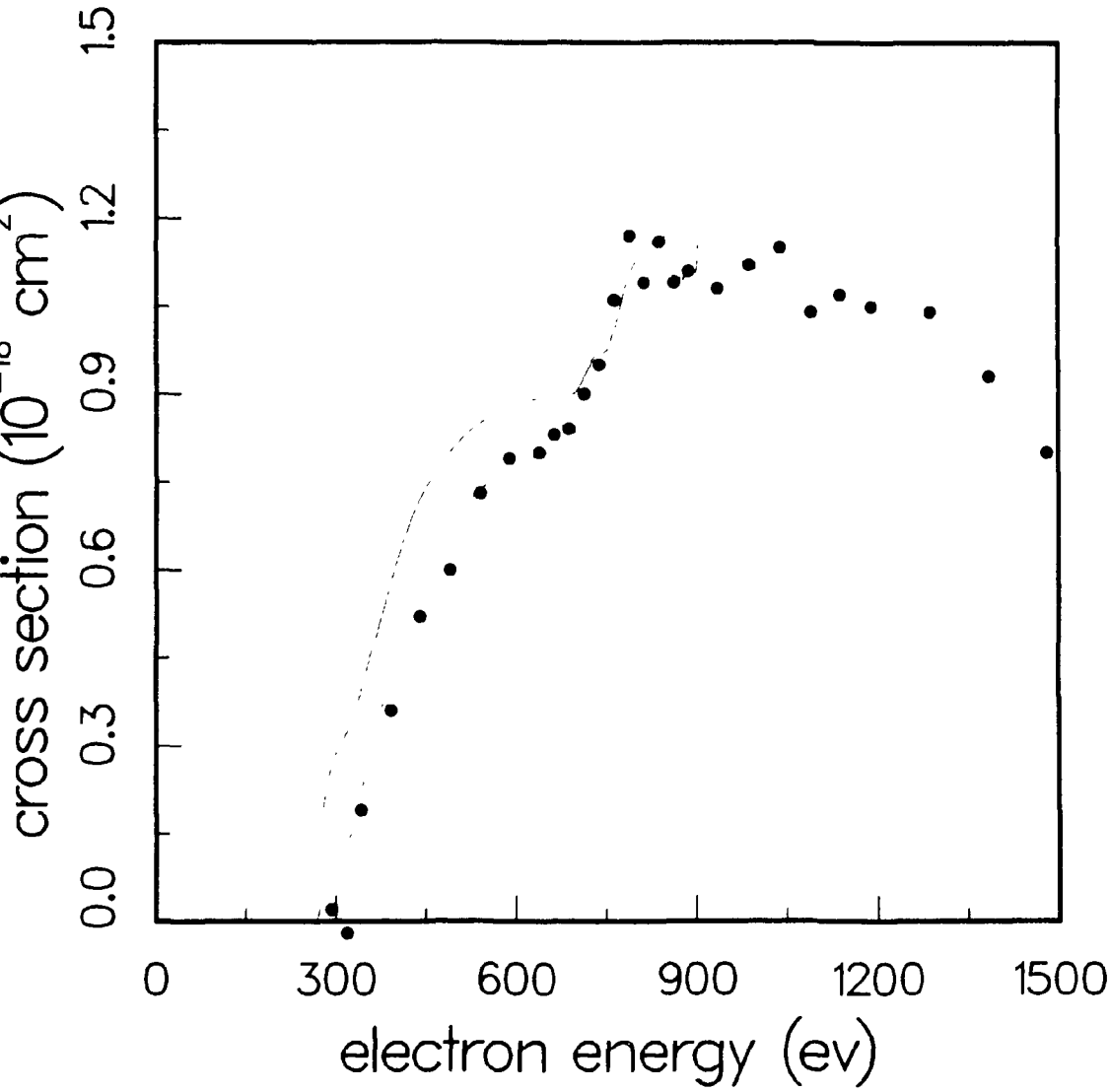

Fig. 17. Electron-impact ionization of Fe^{11+}. Solid curve: total cross section from the $3s^2 3p^2 3d$ excited configuration in the average statistical model; dashed curve: direct cross section only; solid circles: experimental measurements (ref. 8).

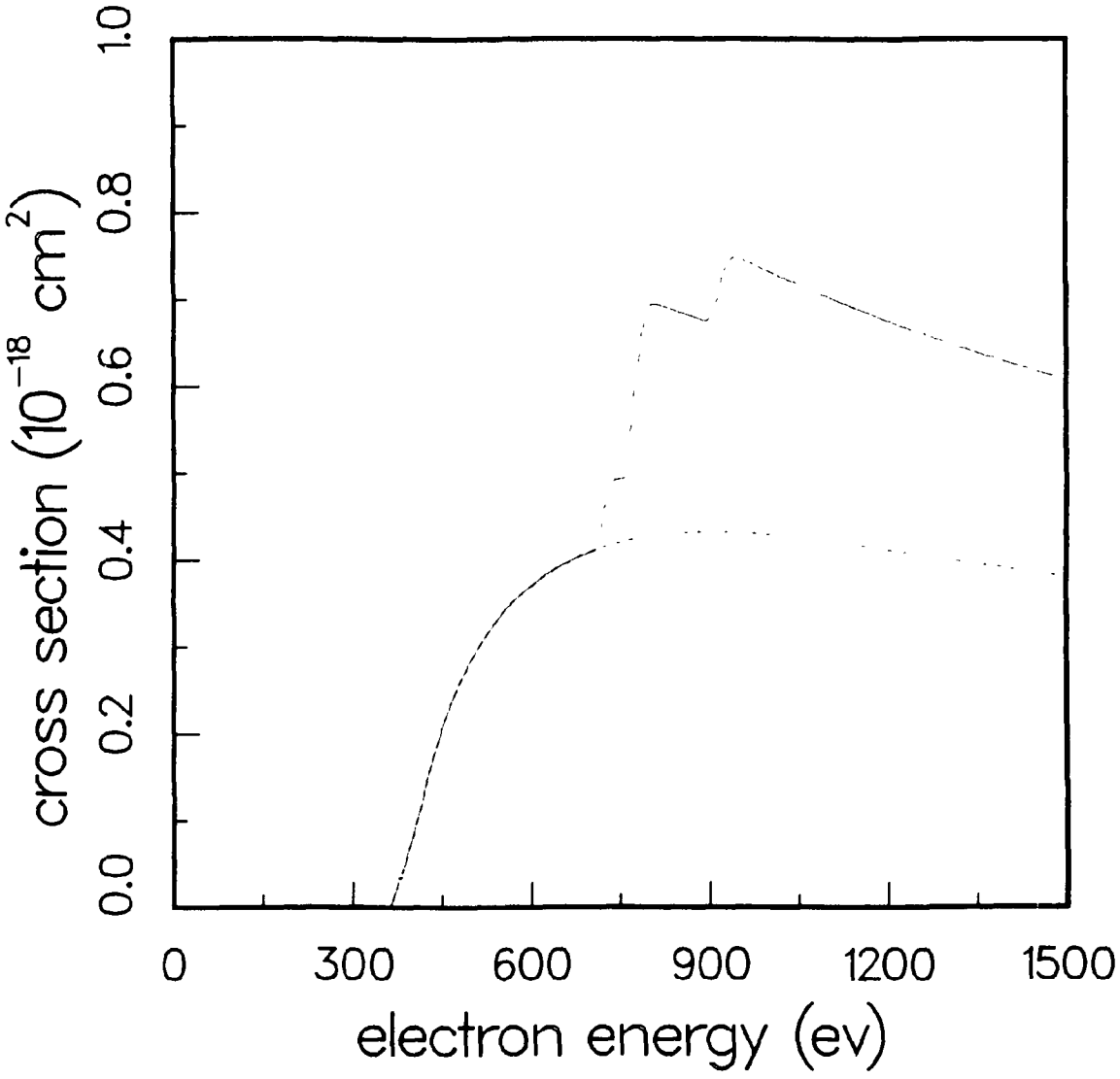

Fig. 18. Electron-impact ionization of Fe^{12+}. Solid curve: total cross section from the $3s^2 3p^2$ ground configuration in the average statistical model; dashed curve: direct cross section only.

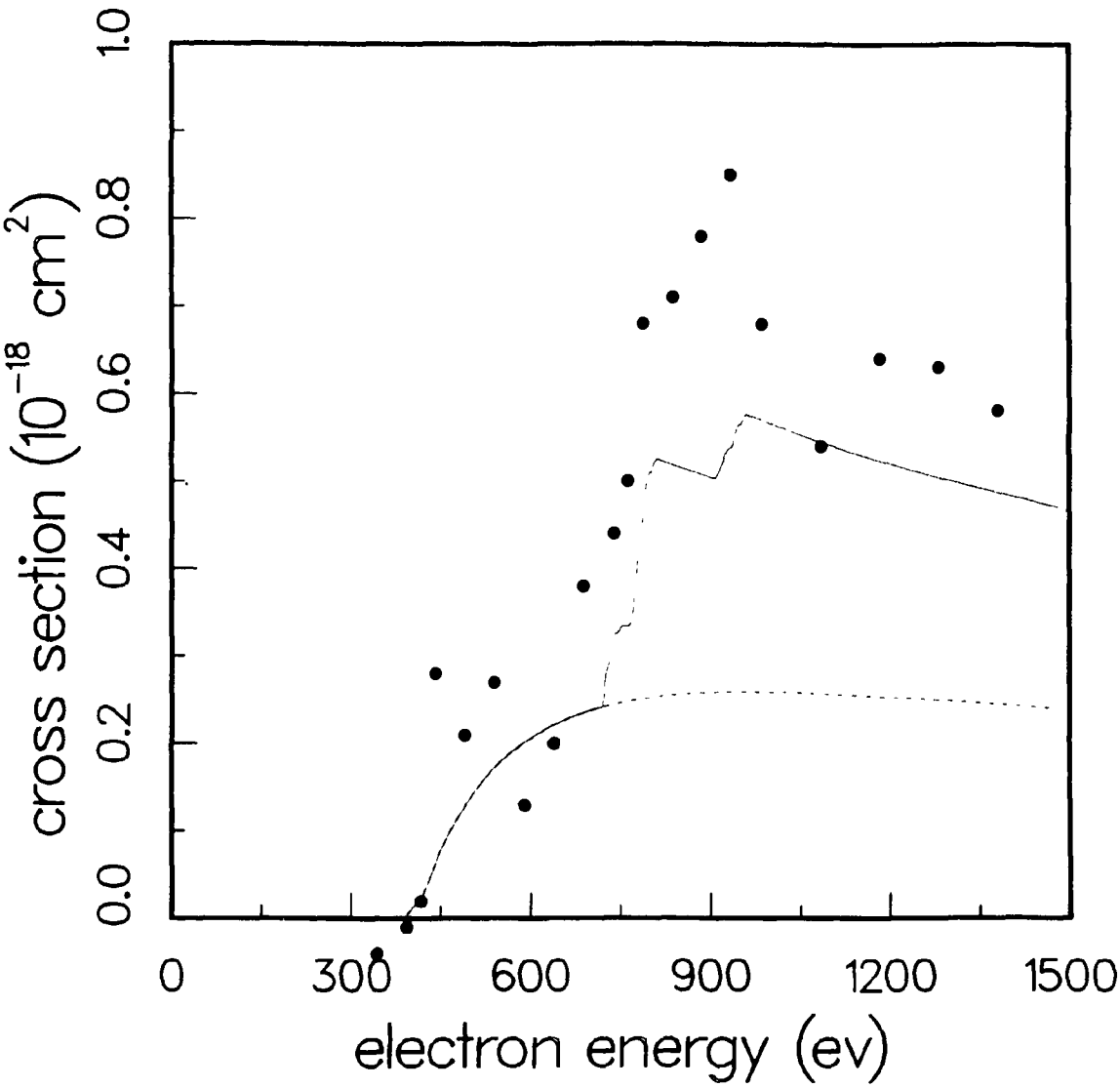

Fig. 19. Electron-impact ionization of Fe^{13+}. Solid curve: total cross section from the $3s^2 3p$ ground configuration in the average statistical model (ref. 19); dashed curve: direct cross section only; solid circles: experimental measurements (ref. 8).

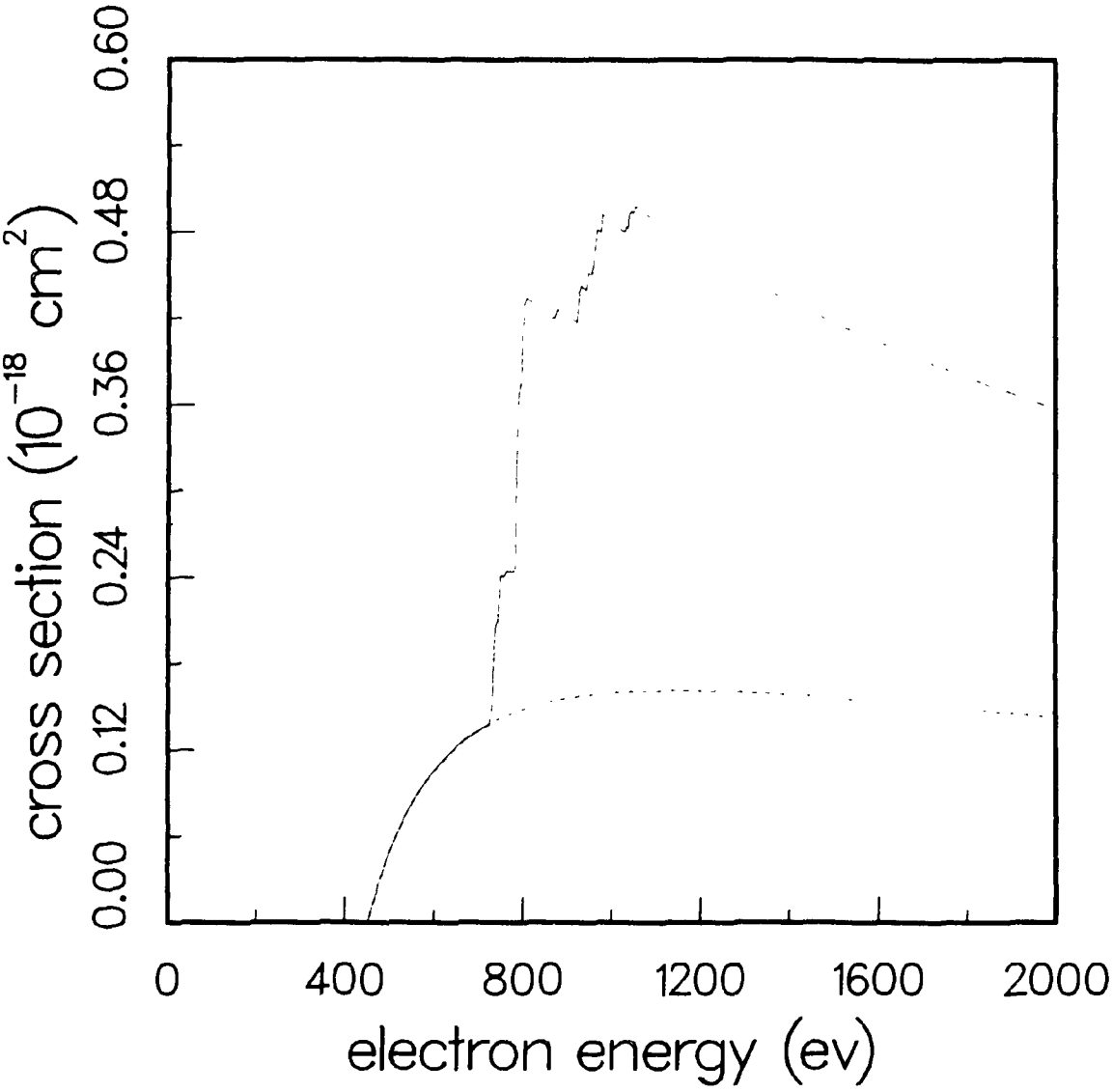

Fig. 20. Electron-impact ionization of Fe^{14+}. Solid curve: total cross section from the $2p^6 3s^2$ ground configuration in the average statistical model; dashed curve: direct cross section only.

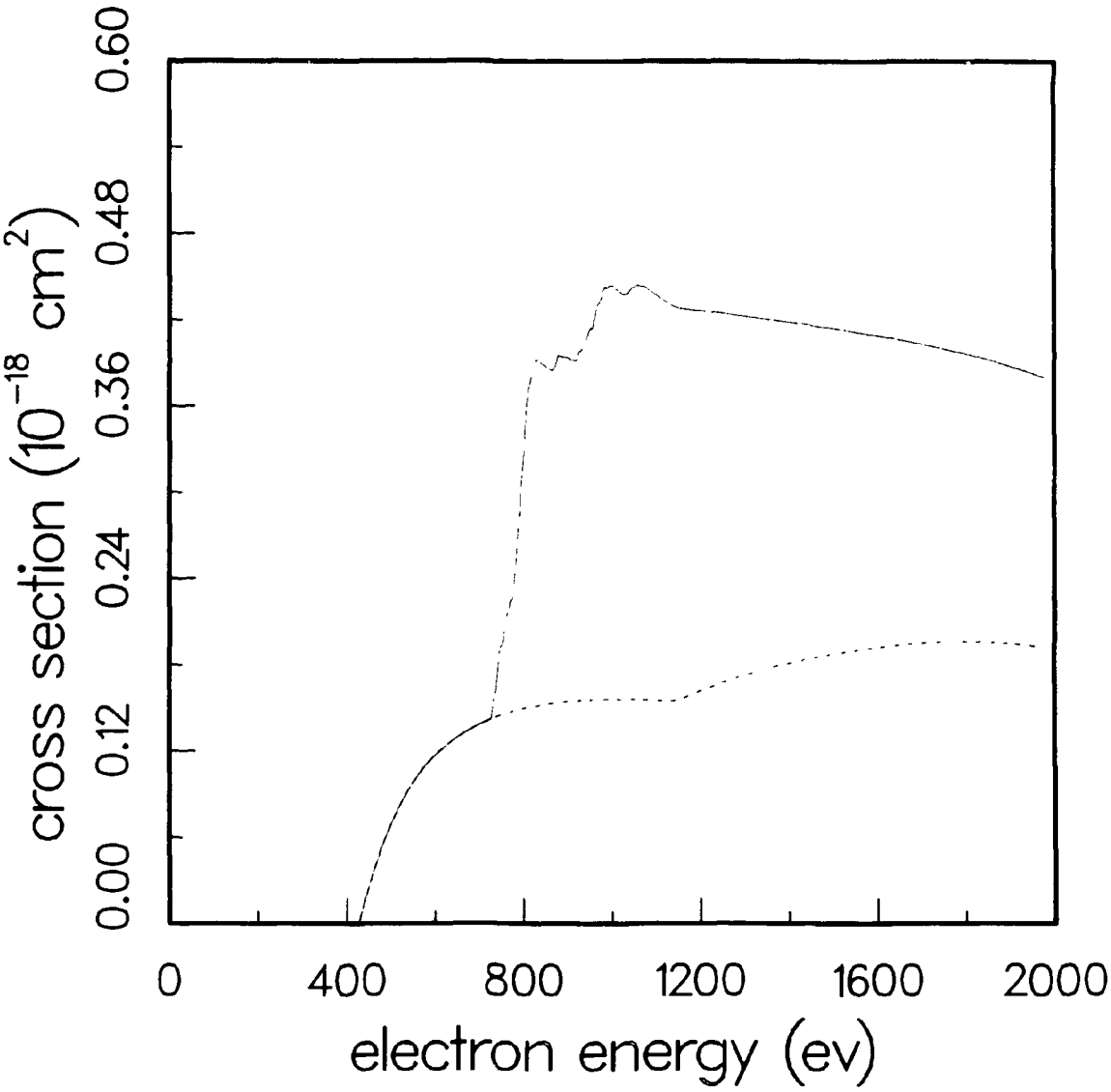

Fig. 21. Electron-impact ionization of Fe^{14+}. Solid curve: total cross section from the $2p^6 3s3p$ excited configuration in the average statistical model; dashed curve: direct cross section only.

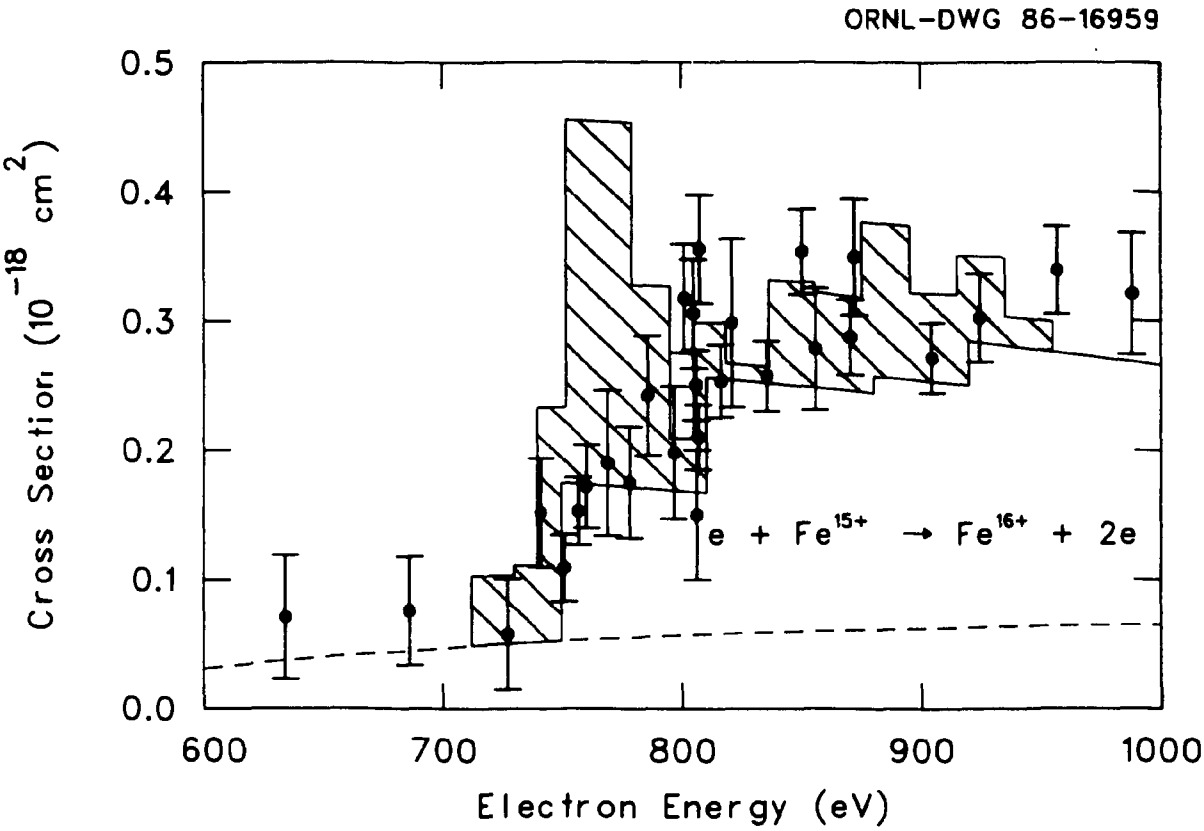

Fig. 22. Electron impact ionization of Fe^{15+}. Lower solid curve: total cross section from the $2p^6 3s$ ground configuration (ref. 20); hatched region includes resonant-recombination double autoionization contribution; dashed curve: direct cross section only; solid circles: experimental measurements (ref. 8).

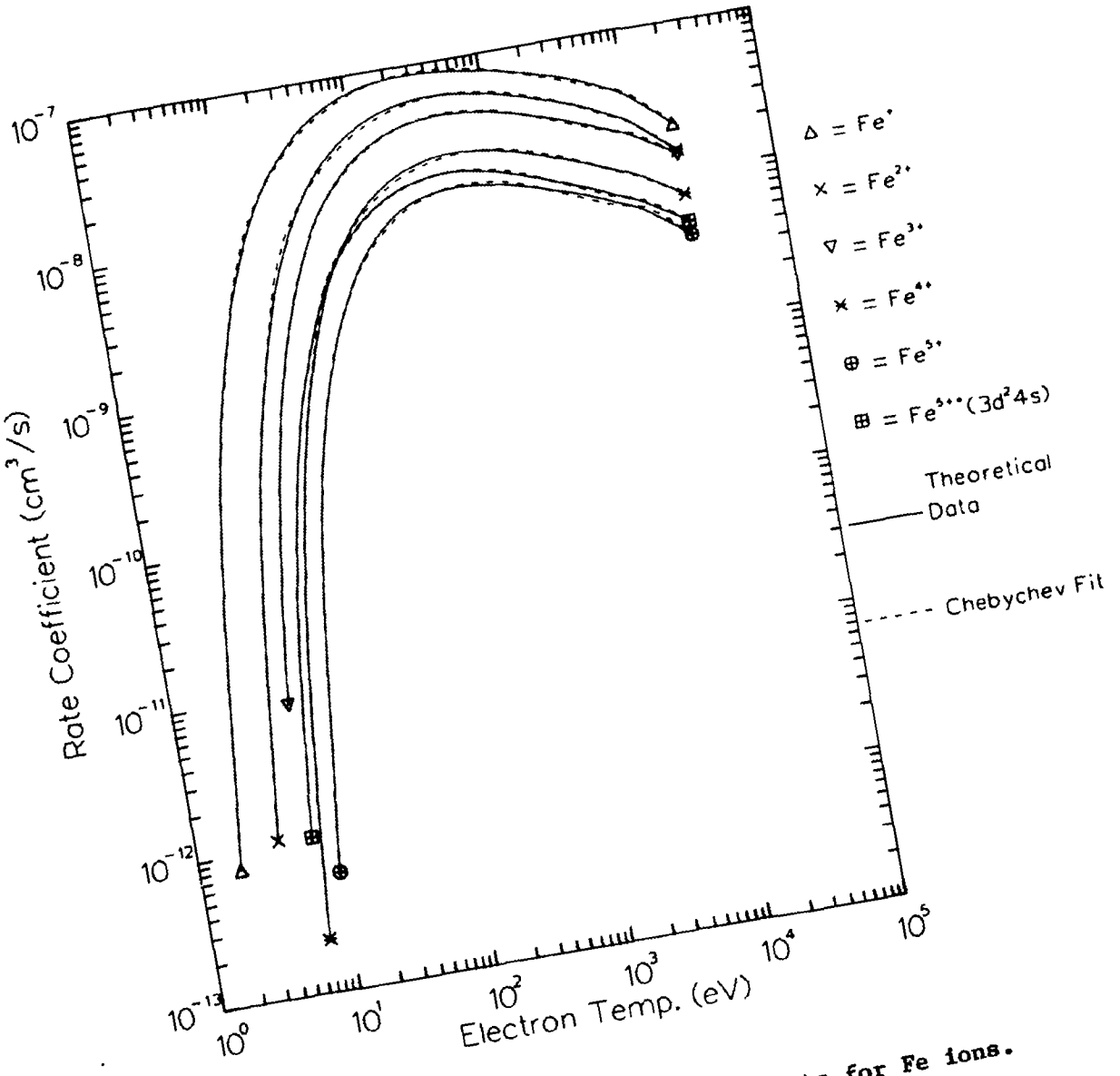

Fig. 23. Theoretical rate coefficients for Fe ions.

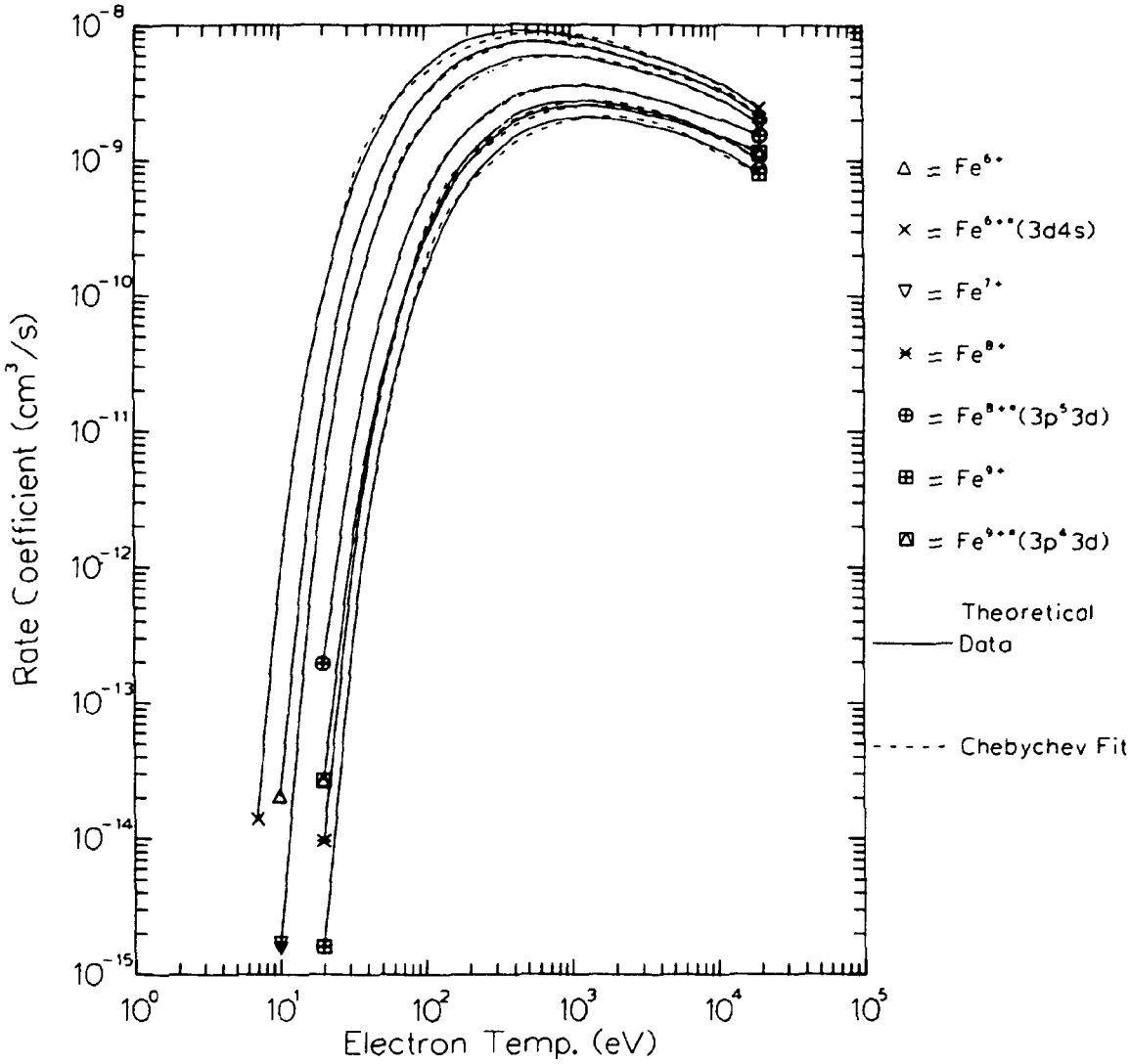

Fig. 24. Theoretical rate coefficients for Fe ions.

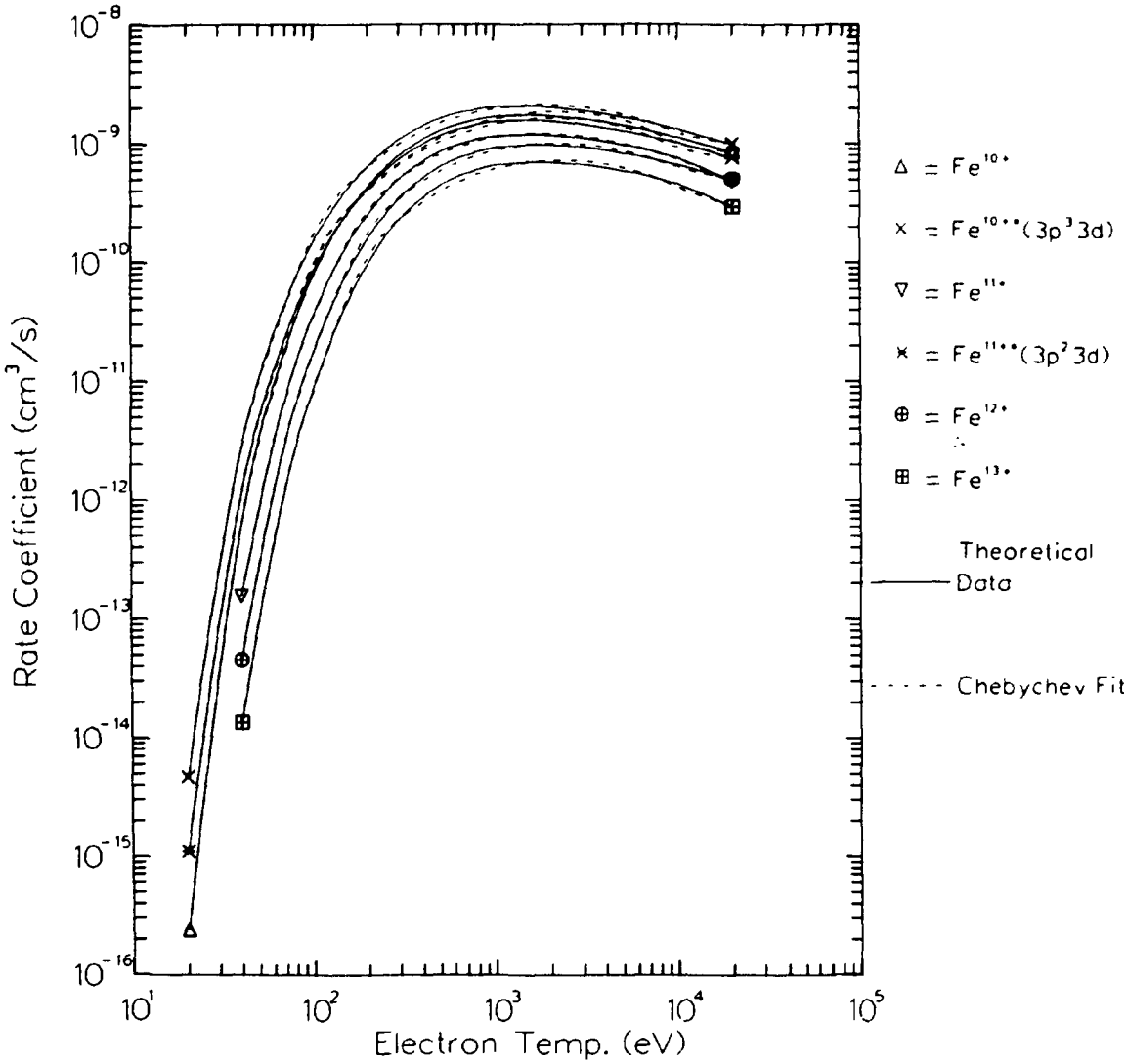

Fig. 25. Theoretical rate coefficients for Fe ions.

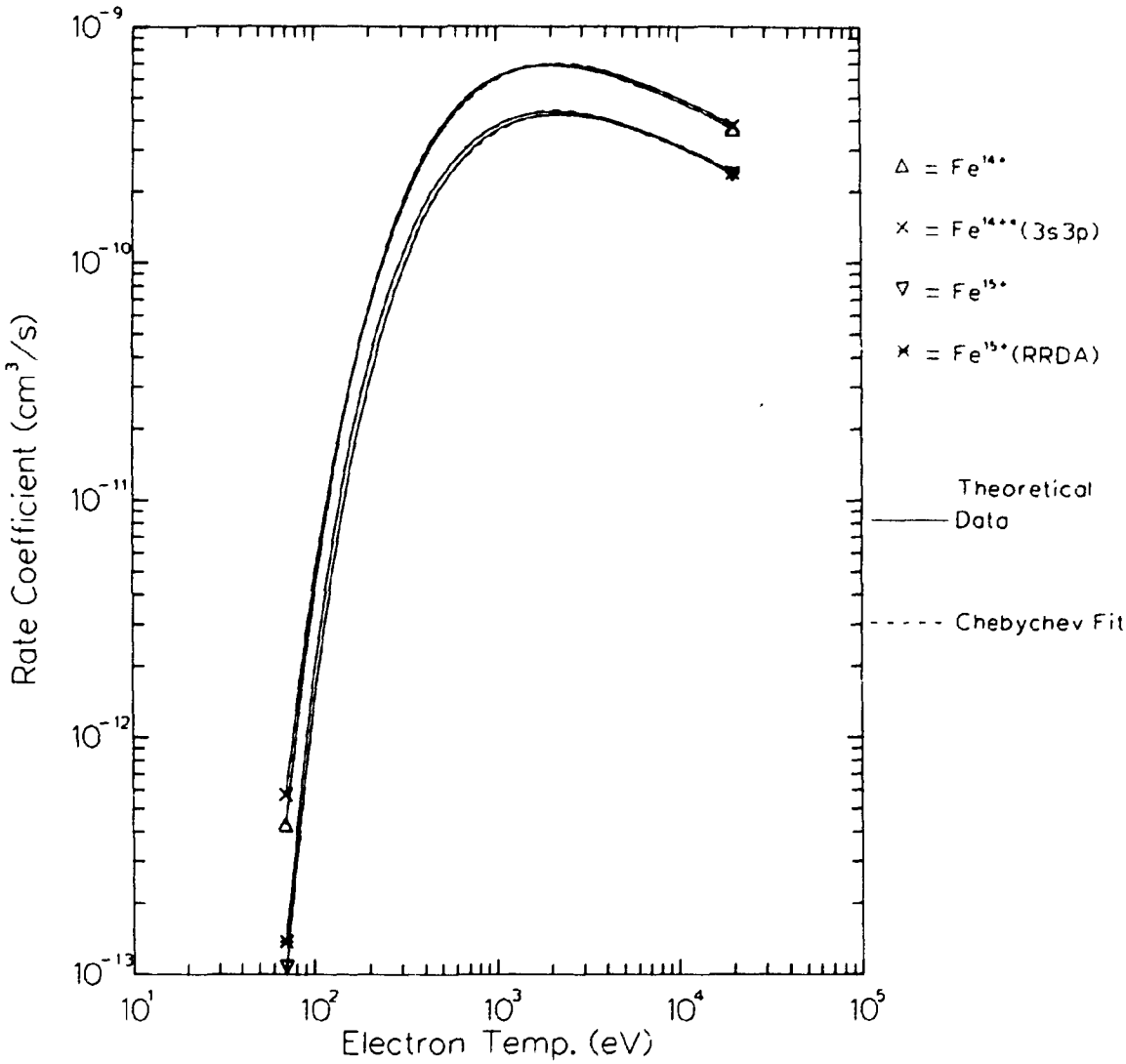

Fig. 26. Theoretical rate coefficients for Fe ions.

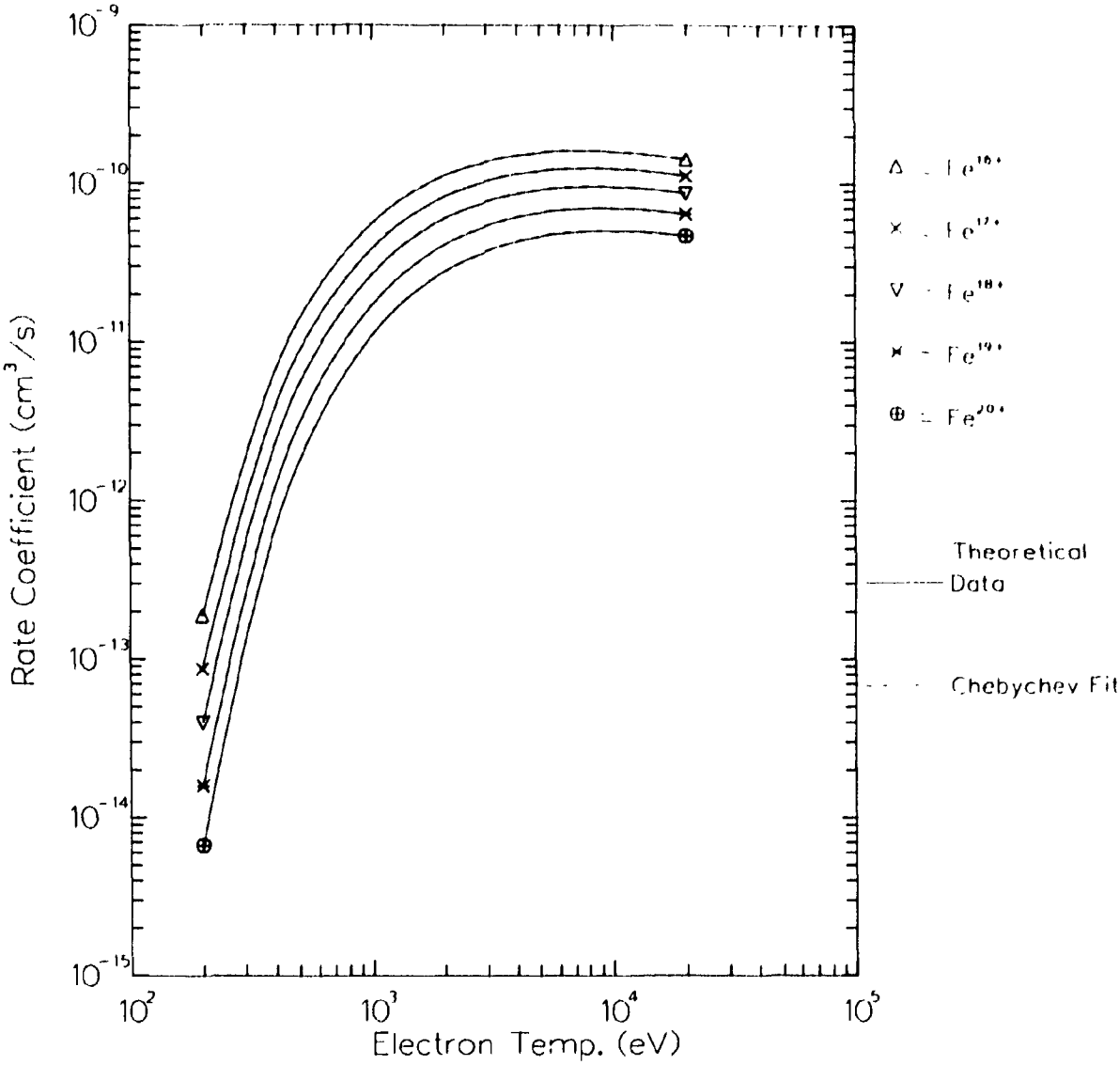

Fig. 27. Theoretical rate coefficients for Fe ions.

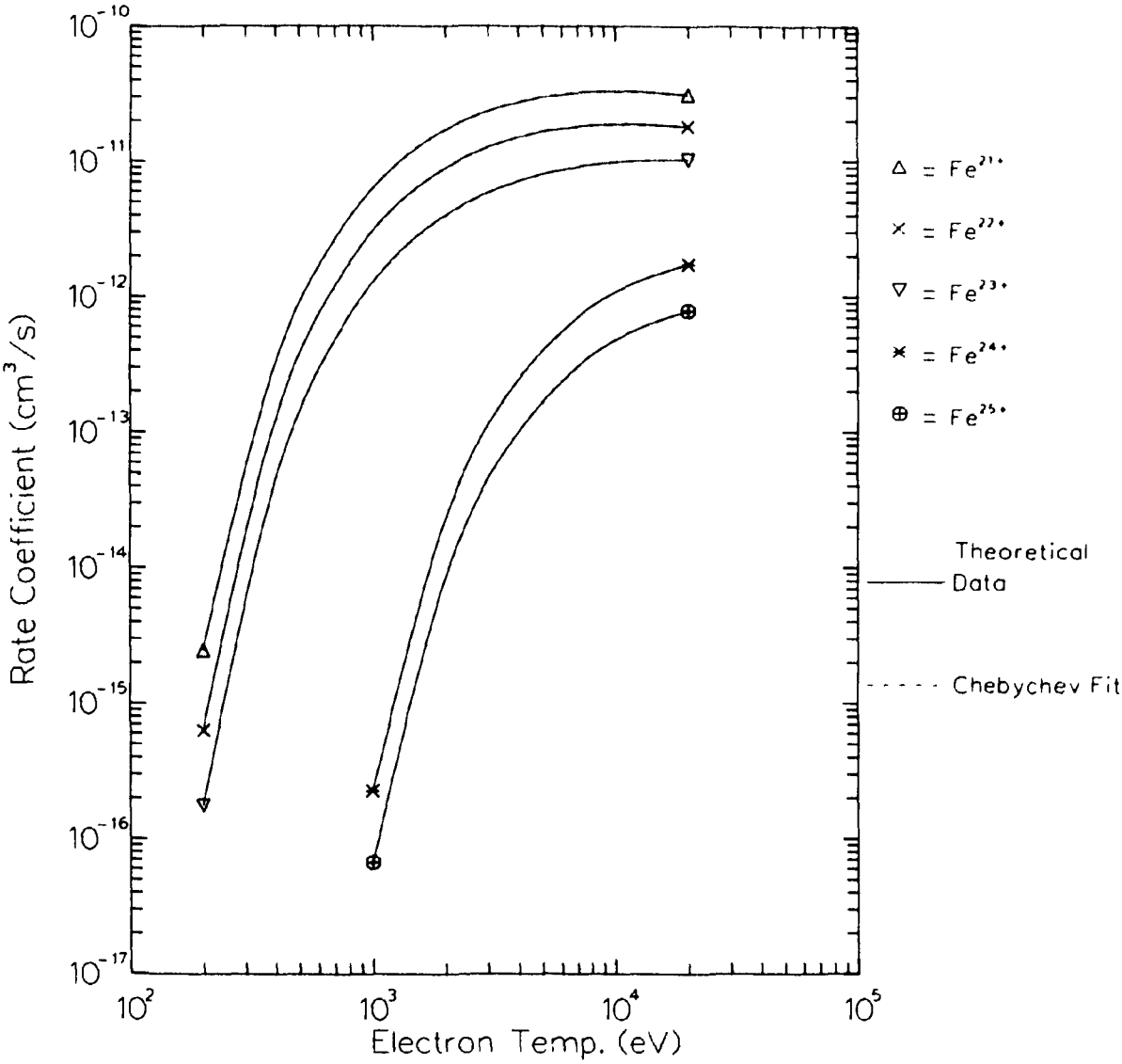

Fig. 28. Theoretical rate coefficients for Fe ions.

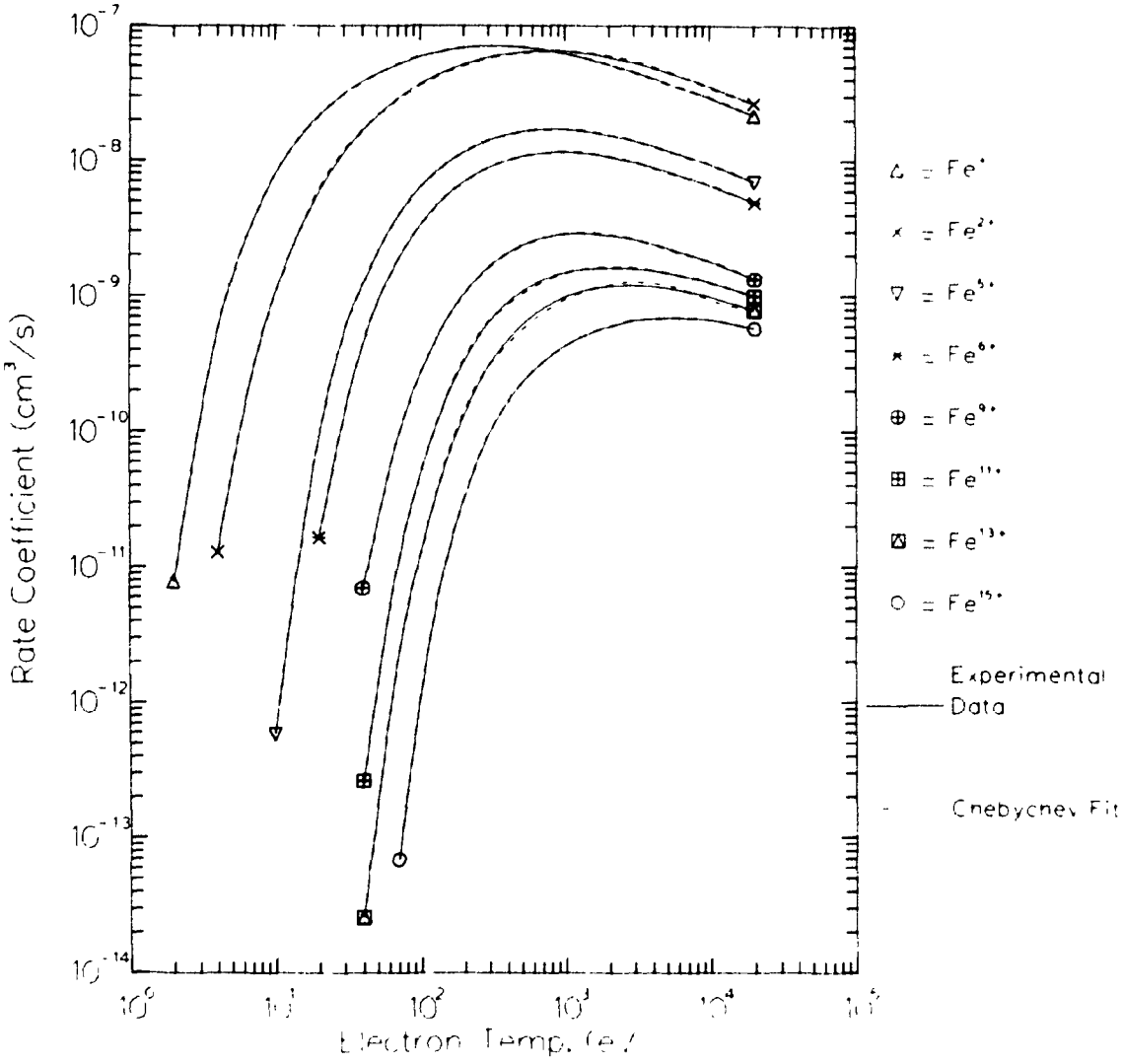

Fig. 29. Experimental rate coefficients for Fe ions.

ORNL/TM-10297

EXTERNAL DISTRIBUTION

1. G. D. Alton
2. C. F. Barnett
3. R. L. Becker
4-8. C. Bottcher
9. E. C. Crume
10. S. Datz
11. P. F. Dittner
12. W. R. Garrett
13. D. C. Gregory
14. C. C. Havener
15. J. T. Hogan
16. H. T. Hunter
17. R. C. Isler
18. C. C. Klepper
19. H. F. Krause
20. F. W. Meyer
21. P. D. Miller
22. P. L. Pepmiller
23. R. A. Phaneuf
24. S. Raman
25. R. K. Richards
26. J. Sheffield
27. C. R. Vane
28-29. Controlled Fusion Atomic Data Center
30. Central Research Library
31. Document Reference Section
32-33. Laboratory Records
34. Laboratory Records, RC
35. ORNL Patent Section
36. Fusion Energy Div. Library
37. Fusion Engineering Design Center

EXTERNAL DISTRIBUTION

38. Office of the Assistant Manager for Energy Research and Development, Department of Energy, Oak Ridge Operations, Box E, Oak Ridge, TN 37831
39. V. A. Abramov, Institute Atommoi Energii, IV Kurchatova, 46 Ulitsa Kurchatova, Moscow D-182, U.S.S.R.
40. V. V. Afrosimov, AF Ioffe Physical-Technical Institute, Leningrad K-21 U.S.S.R. 194021
41. G. Alber, Joint Institute for Laboratory Atrophysics, University of Colorado, Boulder, CO 80309
42. M. Ya. Amusia, AF Ioffe Physico-Technical Institute, Leningrad, U.S.S.R. 194021
43. R. Becker, Institut für Angewandte Physik, Universität Frankfurt, D-6000 Frankfurt/M, Rob.-Mayer Str. 2-4, West Germany
44. Bibliothek, Institut fur Plasmaphysik, KFA, Postfach 1913, D-5170 Julich, Federal Republic of Germany
45. Bibliothek, Max-Planck Institut fur Plasmaphysik, D-8046 Garching bei Munchen, Federal Republic of Germany
46. Bibliotheque, Centre de Recherches en Physique des Plasmas, 21 Avenue des Bains, 1007 Lausanne, Switzerland
47. Bibliotheque, Service due Confinement des Plasma, CEA, B.P. 6, 92 Fontenay-aux-Roses (Seine), France
48. S. L. Bliman, Centre D'Etudes Nucleaires de Grenoble, 85 X Avenue des Martyrs, F-38041 Grenoble, Cedex, France
49. F. Brouillard, Institut de Physique, Chemin du Cyclotron 2, 1348 Louvain-la-Neuve, Belgium
50. A. Burgess, Dept. of Applied Mathematics and Theoretical Physics, Silver Street, Cambridge, CB3 9EW, England

51. P. Burke, Department of Applied Mathematics, Queen's University of Belfast, Belfast BT7 1NN, Northern Ireland
52. J. Callaway, Department of Physics and Astronomy, Louisiana State University, Baton Rouge, LA 70803
53. J. D. Callen, Department of Nuclear Engineering, University of Wisconsin, Madison, WI 53706
54. S. Chantrenne, Lawrence Livermore National Laboratory, P.O. Box 808, Livermore, CA 94550
55. M. Chen, Lawrence Livermore National Laboratory, P.O. Box 808, Livermore, CA 94550
56. A. Chutjian, Jet Propulsion Laboratory, Bldg. 183, Rm. 601, California Institute of Technology, Pasadena, CA 91103
57. C. Cisneros, Instituto de Fisica, Apartado Postal 20-364, Mexico 20, D.F.
58. W. Claeys, Universite Catholique de Louvain, Institut de Physique, Chemin du Cyclotron 2, B-1348, Louvain-la-Neuve, Belgium
59. C. L. Cocke, Department of Physics, Kansas State University, Manhattan, KS 66506
60. L. A. Collins, T-4 MS-212, Los Alamos Scientific Laboratory, Los Alamos, NM 87545
61. R. W. Conn, Department of Chemical, Nuclear, and Thermal Engineering, University of California, Los Angeles, CA 90024
62. R. D. Cowan, T-Division, MS 212, Los Alamos Scientific Laboratory, P.O. Box 1663, Los Alamos, NM 87544
63. D. H. Crandall, ER-542 G-215 GTN, Office of Fusion Energy, U.S. Department of Energy, Washington, DC 20545
64. H. E. Dalhed, L18, Lawrence Livermore National Laboratory, P.O. Box 808, Livermore, CA 94550
65. S. O. Dean, Fusion Energy Development, Science Applications, Inc., 2 Professional Drive, Gaithersburg, MD 20760
66. P. Defrance, University of Louvain, Institut de Physique, B-1348 Louvain la Neuve, Belgium
67. F. J. De Heer, FOM-Institute of Atomic and Molecular Physics, Kruislaan 407, Amsterdam/Watergraafsmeer, The Netherlands
68. Documentation S.I.G.N., Department de la Physique du Plasma et de la Fusion Controlee, Centre d'Etudes Nucleaires, B.P. No. 85, Centre du Tri, 38041 Cedex, Grenoble, France
69. K. T. Dolder, Dept. of Atomic Physics, The University, Newcastle Upon Tyne, England NE1 7RU
70. Bob DuBois, Battelle Northwest, Battelle Blvd., Richland, WA 99352
71. J. Duggan, Department of Physics, North Texas State University, Denton, TX 76203
72. G. H. Dunn, JILA, University of Colorado, Boulder, CO 80309
73. H. Ehrhardt, Fachbereich Physik, Universität Kaiserlautern, D-6750 Kaiserlautern, West Germany
74. G. A. Eliseev, I. V. Kurchatov Institute of Atomic Energy, P.O. Box 3402, 123182 Moscow, U.S.S.R.
75. R. A. Falk, Boeing Aerospace Co., P.O. Box 3999, MS 87-50, Seattle, WA 98124
76. U. Fano, James Franck Institute, Rm. 227, University of Chicago, 5430 Ellis Ave., Chicago, IL 60637

77. J. L. Feldman, Cond. Matter Phys. Branch, Code 6683, U.S. Naval Research Laboratory, Washington, DC 20375
78. C. F. Fischer, Department of Computer Science, P.O. Box 6035, Station B, Vanderbilt University, Nashville, TN 37235
79. H. K. Forsen, Bechtel Group, Inc., Research Engineering, P.O. Box 3965, San Francisco, CA 94105
80. T. F. Gallagher, Physics Department, University of Virginia, Charlottesville, VA 22901
81. S. Geltman, JILA, University of Colorado, Boulder, CO 80309
82. H. B. Gilbody, Department of Pure and Applied Physics, The Queen's University of Belfast, Belfast BT7 1NN, Northern Ireland
83. J. R. Gilleland, GA Technologies, Inc., Fusion and Advanced Technology, P.O. Box 85608, San Diego, CA 92138
84. V. A. Glukhikh, Scientific-Research Institute of Electro-Physical Apparatus, 188631 Leningrad, U.S.S.R.
85. L. B. Golden, Department of Physics, Worthington Scranton Campus, Pennsylvania State University, 120 Ridge View Drive, Dunmore, PA 18512
86. R. W. Gould, Department of Applied Physics, California Institute of Technology, Pasadena, CA 91125
87-91. D. C. Griffin, Physics Department, Rollins College, Winter Park, FL 32789
92. I. W. Griffiths, Royal Society Research Unit, Univ. College of Swansea, Singleton Park, Swansea, United Kingdom
93. R. A. Gross, Plasma Research Laboratory, Columbia University, New York, NY 10027
94. Y. Hahn, Department of Physics, University of Connecticut, Storrs, CT 06268
95. M.F.A. Harrison, Culham Laboratory, Room 131/F7, UKAEA Research Group, Abingdon, Oxfordshire, OX 14 3DB, England
96. A. U. Hazi, Lawrence Livermore National Laboratory, P.O. Box 808, Livermore, CA 94550
97. R.J.W. Henry, Dept. of Physics and Astronomy, Louisiana State University, Baton Rouge, LA 70803
98. A. P. Hickman, Molecular Physics Laboratory, SRI International, Menlo Park, CA 94023
99. E. Hinnov, Plasma Physics Laboratory, Princeton University, Princeton, NJ 08540
100. J. Hiskes, Lawrence Livermore National Lab., Livermore, CA 94550
101. J. G. Hughes, Dept. of Computer Science, Queen's Univ., Belfast, Northern Ireland
102. R. A. Hulse, Plasma Physics Laboratory, Princeton University, P.O. Box 451, Princeton, NJ 08544
103. M. Inokuti, Environmental Research Division, Argonne National Lab., Argonne, IL 60439
104. Y. Itikawa, Institute of Space and Astronautical Science, 6-1, Komaba, Meguro-ku, Tokyo 153, Japan
105. V. L. Jacobs, Plasma Physics Division, Naval Research Laboratory, Washington, DC 20375

106. R. K. Janev, IAEA, Wagramerstrasse 5, P.O. Box 100, A-1400 Vienna, Austria
107. C. J. Joachain, Physique Théorique, Faculté des Sciences, Université Libre de Bruxelles, Code Postal 227, Campus Plaine U.L.B., Boulevand du Triomphe, B-1050, Bruxelles, Belgium
108. Joint Institute for Laboratory Astrophysics, Publications Distribution Center, University of Colorado, Boulder, CO 80309
109. K. W. Jones, Brookhaven National Laboratory, Upton, NY 11973
110. E. Kallne, JET Joint Undertaking, Abingdon, Okon OX14 3EA England
111. Y. Kaneko, Tokyo Metropolitan University, Setagaya-ku, Tokyo, 158, Japan
112. T. Kato, Institute of Plasma Physics, Nagoya University, Nagoya 464, Japan
113. H. P. Kelly, Dept. of Physics, University of Virginia, Charlottesville, VA 22901
114. Y-K. Kim, National Bureau of Standards, Bldg. 221, Washington, DC 20234
115. A. E. Kingston, Department of Applied Mathematics, Queen's University of Belfast, Belfast BT7 1NN, Northern Ireland
116. M. Klapisch, Physics Dept., Racah Institute, Hebrew University, Jerusalem, Israel
117. J. L. Kohl, Center for Astrophysics, 60 Garden Street, Cambridge, MA 02138
118. K. LaGattuta, Physics Dept., University of Connecticut, Storrs, CT 06268
119. Y. T. Lee, Lawrence Livermore National Lab., L-355, P.O. Box 808, Livermore, CA 94550
120. Library, Culham Laboratory, UKAEA, Abingdon, Oxfordshire, OX14 3DB, England
121. Library, FOM Institut voor Plasma-Fysica, Rijnhuizen, Jutphaas, The Netherlands
122. Library, Institute of Physics, Academia Sinica, Beijing, People's Republic of China
123. Library, Institute of Plasma Physics, Nagoya University, Nagoya 464, Japan
124. Library, International Centre for Theoretical Physics, Trieste, Italy
125. Library, Laboratorio Gas Ionizzati, Frascati, Italy
126. Library, Plasma Physics Laboratory, Kyoto University, Gokasho Uji, Kyoto, Japan
127. A. Lorenz, IAEA, Wagramerstrasse 5, P.O. Box 100, A-1400 Vienna, Austria
128. J. B. Mann, Los Alamos Scientific Laboratory, P.O. Box 1663, Los Alamos, NM 86544
129. M.R.C. McDowell, Dept. of Mathematics, Royal Holloway College, Egham, Surrey TW20 0EX, England
130. E. J. McGuire, Sandia Labs, Orgn. 1231, Albuquerque, NM 87115
131. D. M. Meade, Plasma Physics Laboratory, Princeton University, P.O. Box 451, Princeton, NJ 08544
132. W. Mehlhorn, Fakultät für Physik, Universität Freiburg, D-78 Freiburg, Federal Republic of Germany

133. A. L. Merts, T-4, MS 212, Los Alamos National Laboratory, Los Alamos, NM 87544
134. D. R. Mikkelsen, Plasma Physics Lab., P.O. Box 451, Princeton, NJ 08544
135. J.B.A. Mitchell, Physics Dept., Univ. Western Ontario, London, Ontario, Canada N6A5B9
136. D. L. Moores, Dept. of Physics and Astronomy, University College London, Gower Street, London WC1E 6BT, United Kingdom
137. T. J. Morgan, Department of Physics, Wesleyan University, Middletown, CT 06457
138. W. L. Morgan, Lawrence Livermore National Laboratory, L-18, P.O. Box 808, Livermore, CA 94550
139. R. L. Morse, Department of Physics, University of Arizona, Tucson, AZ 85721
140. A. Msezane, Department of Physics, Morehouse College, 233 Chestnut Street SW, Atlanta, GA 30314
141. D. Mueller, Fakultäte für Physik, Universitäte Bielefeld, Postfach 8640, 4800 Bielefeld 1, West Germany
142. A. Müller, Strahlenzentrum Justus Liebig University., Leihgesterner Weg 217, D-6300 Giessen, W. Germany
143. D. W. Norcross, JILA, University of Colorado, Boulder, CO 80309
144. S. Ohtani, Institute of Plasma Physics, Nagoya University, Nagoya 464, Japan
145. R. E. Olson, Physics Department, University of Missouri-Rolla, Rolla, MO 65401
146. B. Peart, Dept. of Atomic Physics, The University, Newcastle Upon Tyne, England NE1 7RU
147. J. M. Peek, Group T-4, MS-B212, Los Alamos National Laboratory, Los Alamos, NM 87545
148-152. M. S. Pindzola, Physics Department, Auburn University, Auburn, AL 36849
153. Plasma Research Laboratory, Australian National University, P.O. Box 4, Canberra, A.C.T. 2000, Australia
154. D. E. Post, Jr., Princeton Plasma Physics Lab., P.O. Box 451, Princeton, NJ 08544
155. A. Pradhan, JILA, University of Colorado, Boulder, CO 80309
156. R. V. Pyle, Magnetic Fusion Group, Lawrence Berkeley Laboratory, University of California, Berkeley, CA 94720
157. J. F. Reading, Physics Department, Texas A&M University, College Station, TX 77840
158. P. J. Reardon, Brookhaven National Laboratory, Upton, NY 11973
159. J. R. Roberts, A 59-221, National Bureau of Standards, Washington, DC 20234
160. L. Roszman, National Bureau of Standards, Washington, DC 20234
161. W. L. Rowan, Fusion Research Center, Univ. of Texas, Austin, TX 78712
162. D. D. Ryutov, Institute of Nuclear Physics, Siberian Branch of the Academy of Sciences of the U.S.S.R., Sovetskaya St. 5, 630090 Novosibirsk, U.S.S.R.

163. E. Salzborn, Strahlenzentrum, Justus Liebig University, Leihgesterner Weg 217, D-6300 Giessen, West Germany
164. D. H. Sampson, 505 Davey Laboratory, Pennsylvania State University, University Park, PA 16802
165. M. J. Seaton, Department of Physics, University College London, Gower Street, London WC1 6BT, England
166. A.C.H. Smith, Dept. of Physics and Astronomy, University College London, London WC1E 6BT, England
167. J. J. Smith, IAEA, Wagramerstrasse 5, P.O. Box 100, A-1400 Vienna, Austria
168. I. Spighel, Lebedev Physical Institute, Leninsky Prospect 53, 117924 Moscow, U.S.S.R.
169. R. Srivastava, Department of Physics, University of Roorkee, Roorkee 247672, India
170. W. M. Stacey, Jr., School of Nuclear Engineering, Georgia Institute of Technology, Atlanta, GA 30332
171. D. Steiner, Rensselaer Polytechnic Institute, Troy, NY 12181
172. B. Stratton, Princeton Plasma Physics Laboratory, P.O. Box 451, Princeton, NJ 08544
173. H. Tawara, Institute of Plasma Physics, Nagoya University, Nagoya 464, Japan
174. H. Taylor, Chemistry Department, University of Southern California, University Park, Los Angeles, CA 90007
175. A. Temkin, Atomic Physics Office, Code 680.1, Goddard Space Flight Center, Greenbelt, MD 20771
176. Thermonuclear Library, Japan Atomic Energy Research Institute, Tokai, Naka, Ibaraki, Japan
177. V. T. Tolok, Kharkov Physical-Technical Institute, Academical St. 1, 310108 Kharkov, U.S.S.R.
178. R. Varma, Physical Research Laboratory, Navrangpura, Ahmedabad, India
179. E. Wahlin, JILA, University of Colorado, Boulder, CO 80309
180. J. F. Williams, Physics Department, University of Western Australia, Perth 6009, Australia
181-305. Given distribution as shown in TIC-4500 under UC-20f, MFE-Experimental Plasma Physics